School of Mathematics & Statistics

MMath Project

Particle Dynamics of Matter-Wave Solitons

Author:
Imogen Large

Supervisor:
Dr. Nick Parker

May 2014

Abstract

Solitons are important in the modelling of nonlinear systems like black holes and fibre-optics, however due to their non-dispersive nature they are difficult to form in practical experiments. Bose-Einstein condensation provides a physical system in which solitons can be observed and controlled. To a good approximation the Gross-Pitaevskii equation calculates the dynamics of a Bose-Einstein condensate theoretically, and an exact soliton solution can be derived. In this dissertation, Hamiltonian mechanics are used to provide a particle model for various soliton systems. In recent experiments, a Gaussian barrier was introduced into the trapping potential of a one-soliton system; here the system is modelled theoretically and the results show excellent agreement. Two external potentials are considered in two-soliton systems; the typical interaction potential between solitons demonstrates the phase-shift, and the Lennard-Jones potential considers the attractive and repulsive forces between solitons. The contrasting nature of these potentials is observed through simulation and presented in Poincaré sections.

Contents

Chapter 1

Introduction

1.1 Solitons

Solitons, or solitary waves, are localised wave-packets which do not disperse over time. A regular wave disperses as it propagates and its amplitude decreases; in contrast a solitary wave retains a fixed height and shape despite propagation. Solitons are solutions to nonlinear wave equations describing particle-like waves of energy which are precise and rigorous. Solitary waves are experimental representations of these solutions, and so can be considered as approximate forms of the analytical solutions. Solitary waves can be applied in the analysis of various nonlinear systems such as nonlinear optics and shallow water.

Solitons were first observed by John Scott Russell, a civil engineer and naval architect, in 1834 on the Union Canal near Edinburgh. He was investigating the most efficient design of canal boats when the boat he was observing came to a sudden stop, and the wave at the front of the boat carried on moving. Russell pursued the wave and this extract from his report details his findings:

"I believe that I shall best introduce this phenomenon by describing the circumstances of my own first acquaintance with it. I was observing the motion of a boat which was rapidly drawn along a narrow channel by a pair of horses, when the boat suddenly stopped - not so the mass of water in the channel which it had put in motion; it accumulated round the prow of the vessel in a state of violent agitation, then suddenly leaving it behind, rolled forward with great velocity, assuming the form of a large solitary elevation, a rounded, smooth and well-defined heap of water, which continued its course along the channel apparently without change of form or diminution of speed. I followed it on horseback, and overtook it still rolling on at a rate of some eight or nine miles an hour, preserving its original figure some thirty feet long and a foot to a foot and a half in height. Its height gradually diminished, and after a chase of one or two miles I lost it in the windings of the channel. Such, in the month of August 1834, was my first chance interview with that singular and beautiful phenomenon which I have called the Wave of Translation, a name which it now very generally bears." [1]

The "Wave of Translation" witnessed by Russell did not decrease in height or speed but continued to propagate with its original profile. This gives reason for us to believe he did indeed observe a soliton. Russell continued his investigations into the "beautiful phenomenon", recreating the wave using a plate which formed a division across a long narrow channel of shallow water [1]. Russell [2] extracted some essential properties of the wave of translation, two of which are

- *"the higher wave moves more rapidly than the lower"* and
- *"the great primary waves of translation cross each other without change of any kind"*.

Precise definitions of solitons are difficult to find, and therefore, in this report, we define solitons based on properties given by Drazin and Johnson [3]. A soliton is any solution of a nonlinear equation (or system) which (i) represents a wave of permanent form; (ii) is localised, so that it decays or approaches a constant at infinity; (iii) can interact strongly with other solitons and retain its identity.

The crucial feature is that these waves interact strongly and then continue to propagate with almost no interaction. We consider a system of two solitons of different amplitudes travelling in the same direction [4]. They are placed with sufficient gap between them such that their tails don't overlap. As the taller wave catches up with the shorter one, we may have expected the waves to combine in some way but this is not the case. Both solitons emerge unchanged from the interaction. They both retain their form, amplitude and speed and there is a slight shift in position. This property is more comparable to that of a particle. This gives the wave particle-like characteristics, emphasised when Zabusky and Kruskal [5] named the waves 'solitons' (after protons, photons, etc.).

1.1.1 Wave Equations

We consider the classical wave equation,

$$u_{tt} - c^2 u_{xx} = 0 \tag{1.1}$$

where $u(x,t)$ is the amplitude of the wave, c is a constant with $c > 0$ and the subscript denotes the partial derivative. Equation (1.1) is a linear wave equation which describes a wave propagating in a vacuum without dissipative effects. The wave disperses as it propagates. We wish to describe a wave without dispersion and so look to include nonlinearities which balance the dispersive effects.

As discovered by John Scott Russell, solitons have been seen and reproduced in shallow water dynamics. In 1895, Korteweg and de-Vries [6] derived this equation to describe these waves,

$$u_t + (1+u)u_x + u_{xxx} = 0. \tag{1.2}$$

which includes a nonlinearity in its simplest form and is known as the KdV equation. The nonlinear partial differential equation can be solved using the inverse scattering transform. This method can be applied to nonlinear integrable systems and used to give exact solutions.

Travelling waves in shallow water are described such that the top of the peak is travelling faster than the bottom. This causes the wave to break. Korteweg and de-Vries were interested in exploring if long water waves continued to *"steepen in front and become less steep behind"* [4]. They showed that the KdV equation has steady progressing wave solutions,

$$u(x,t) = -\frac{1}{2}a^2 \operatorname{sech}^2\left[\frac{1}{2}a\left(x - x_0 - a^2 t\right)\right]. \tag{1.3}$$

The velocity a^2 is proportional to the amplitude. The width is inversely proportional to the square root of the amplitude. Thus we know that taller solitary waves travel faster and are narrower than shorter ones [4], confirming the characteristic given by Russell [2].

Another nonlinear model that supports soliton solutions, more relevant to our study, is the nonlinear Schrödinger Equation. Originally arising in the theory of superconductivity and later in the theory of superfluidity [3], the NLS equation is given by

$$iu_t + \frac{1}{2}u_{xx} + |u|^2 u = 0. \tag{1.4}$$

Like the KdV equation, the NLS equation can be applied to packets of water waves and additionally plasma waves. The most important applications of the NLS equation is in the field of nonlinear optics. It was first suggested in 1973 that optical fibres could support solitons pulses [7,8]. At the time, fibre optics research was focussed on reducing the levels of information lost over large distances and solitons offered a solution [9]. Since then solitons have proved crucial in preserving a signal through fibre optics. The NLS equation is relevant for modelling solitons in Bose-Einstein condensates which we explore further in this dissertation.

1.2 Solitons in Bose-Einstein Condensates

1.2.1 Quantum Particles and Wave-Particle Duality

The dynamics of everyday objects around us can be modelled by classical mechanics however this is not sufficient for particles or objects of such a tiny scale. The behaviour of quantum particles is subject to quantum mechanics which provides a framework for describing dynamics at the subatomic lengthscale. Heisenburg's uncertainty principle states that it is not possible to know the position and velocity of a particle simultaneously [10], and therefore the position and velocity of quantum particles are each defined by a probability distribution. This uncertainty gives the particles a degree of 'blurriness' as their exact positions and velocities are not known. The 'blurriness' in position is described by the de Broglie wavelength, λ_{dB}. Since quantum particles are defined to have this wavelength, they possess the properties of waves as well as particles; this is called wave-particle duality.

All particles can be classified as either bosons or fermions. The distinction is important because, due to their distinguishing properties, the behaviour of a gas of bosons differs greatly from fermionic gases. Bosons are particles with integer spin (with angular momentum 0, 1, 2, 3, ...); fermions have half-integer spin ($1/2$, $3/2$, $5/2$, ...) [11]. Examples of fermions include fundamental particles, electrons, neutrons and protons. Fermions cannot occupy the same quantum state at the same time; they are unsociable. Combining an even number of fermions forms a composite particle with integer spin, a boson. Photons and the majority of atoms are examples of bosons. Bosons are able to occupy the same quantum state and are sociable in nature. The solitons described in this dissertation are produced in a gas which exploits the social nature of bosons.

1.2.2 Bose-Einstein Condensates

A quantum gas is a gas where quantum mechanics rather than Newtonian mechanics dominates the behaviour of the particles. Quantum gases are formed at cold temperatures, at less than 1 millionth of a degree above absolute zero (0 Kelvin (K) or -273°C).

Einstein [12] was interested in how the sociable nature of the bosons could be applied and first theorised a quantum mechanical phenomenon called Bose-Einstein condensation in 1925 using Bose's newly theorised statistics for quantum particles. It wasn't until 1995 that it was realised in weakly interacting atomic gases [13].

Consider a system of a fixed number of atoms with a fixed total energy. The sociable boson property allows the atoms to be in any state within the system. The particles have an average separation d and velocity $\mathbf{v}$.

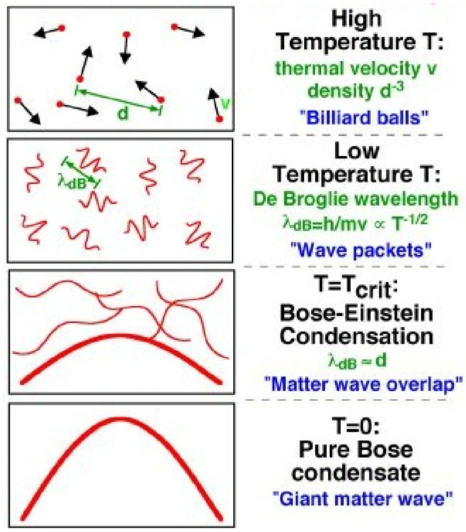

Figure 1.1: The diagram explains criterion for Bose-Einstein condensation [14].

At relatively high temperatures the particles move around randomly with high velocities, bouncing off each other like snooker balls and d is large, as shown in the first panel of Figure 1.1. If or when they collide, the particles behave classically. The temperature decreases and the particles begin to behave more like waves (panel 2). Each wave-packet is localised with a size given by the de Broglie wavelength,

$$\lambda_{dB} = \frac{h}{m|\mathbf{v}|} \propto T^{-1/2}, \tag{1.5}$$

where $h \approx 6.67 \times 10^{-34}$Js is Planck's constant, m is the mass of the particle, $\mathbf{v}$ is the velocity and T is the temperature of the system. The temperature decreases, tending towards absolute zero, and the particles are moving slower. As $|\mathbf{v}| \to 0$, the wavelengths of each particle increases. As the gas is cooled the number of atoms in the lowest energy state of the system gets bigger. When the system reaches a critical temperature, T_C, the size of the wave-packets increases to the extent that $\lambda_{dB} \approx d$, and the particles start to overlap, as shown in panel 3. As they overlap they combine to form a giant matter wave across the whole system. Within the huge wave individual particles can no longer be identified and the atoms behave as one. At $T = T_C$ the number of particles in the lowest energy state increases significantly forming a spike in the energy distribution, see Figure 1.2. This is a Bose-Einstein condensate. At $T = 0$ all the particles fall into the ground energy state and this is a pure Bose-Einstein condensate, depicted in the final panel of Figure 1.1.

Bose-Einstein condensation can occur in other scenarios. The condensation occurs when the wave-packets overlap. This happens either at very low temperatures (as detailed above) or at very high densities. An example of the second case is neutron stars where the density of particles is so great that the particles are forced so close together that they overlap.

Quantum physics, due to its definition, is too small to be observed easily. Bose-Einstein condensation offers the chance to view particles conforming to quantum mechanics on a larger scale. In the current pursuit of the quantum 'era', manipulation of BECs is crucial to the progress

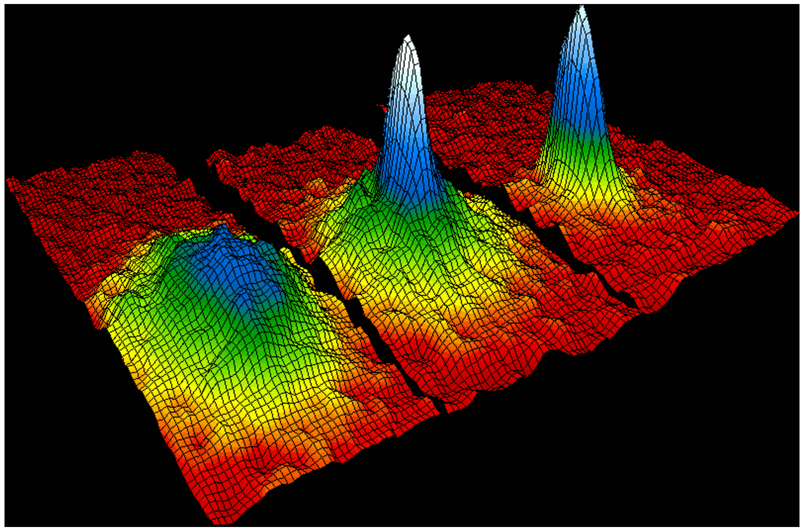

Figure 1.2: First weakly interacting atomic Bose-Einstein Condensate realisation by Cornell *et al.* [11] who received a Nobel Prize in Physics 2001.

of this research. BECs are nonlinear systems; this is important as it provides a platform to investigate nonlinear objects such as investigate solitons.

1.2.3 Solitons in Bose-Einstein Condensates

Solitons arise in BECs in two forms which is determined by atomic interactions within the condensate [15]. The interactions introduce the nonlinearity into the system which balances the dispersion. In the absence of interactions, there is no nonlinearity and therefore no soliton in the condensate.

The particles in the BEC have a weak interaction between each other which is only felt when they are close together. The interaction is still effective, despite the weakness, due to the very cold temperatures and very low energy in the system. The consequence of the atoms being so close together is an energetic cost for the interaction, g, defined as

$$g = \frac{4\pi\hbar^2 a_s}{m}, \tag{1.6}$$

where $\hbar$ is reduced Planck's constant, a_s is the s-wave scattering length and m is the mass of each atom. The scattering length is the critical distance between the atoms when an interaction occurs. Experimentalists can control the magnitude and sign of a_s and therefore g, and so can determine the interactions between the atoms.

- $g > 0$: repulsive interactions; it costs the system energy to keep the atoms close together.
- $g = 0$: no interactions and no nonlinearity.
- $g < 0$: attractive interactions; it reduces the energy in the system as the atoms are already close together.

Formed in a BEC with repulsive interactions, dark solitons are localised, negative dips in amplitude which satisfy the defining properties of solitons [3]. Contrastingly bright solitons appear in BECs with attractive interactions. They are localised bumps in the condensate similar to pulses of light. The attractive interactions allow the bright soliton to retain its profile without dispersing despite propagation. In this dissertation, we consider bright solitons in Bose-Einstein condensates with attractive atomic interactions. Being able to control the interactions within the BEC allows systems to be constructed that are advantageous for modelling nonlinear systems like solitons. Solitons can be studied experimentally in systems of water or optics, but the unique properties of the BECs allow the solitons to last indefinately.

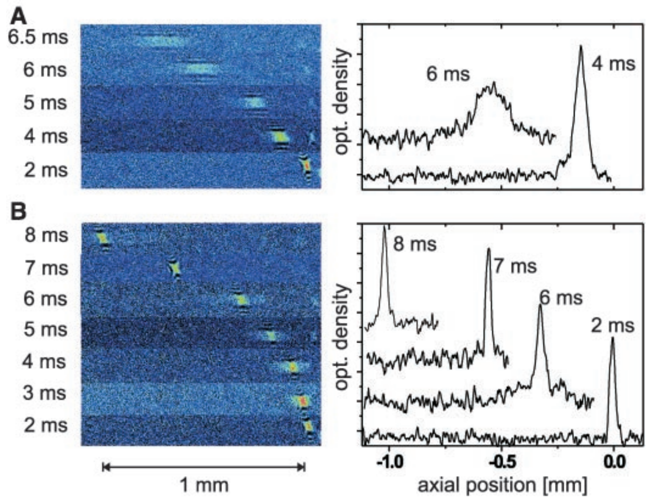

Figure 1.3: Matter-wave bright soliton as produced by Khaykovich *et al.* [16]. Panel A shows a system with $g = 0$, and the soliton disperses. Panel B is a system with attractive interactions and the profile of the soliton is maintained.

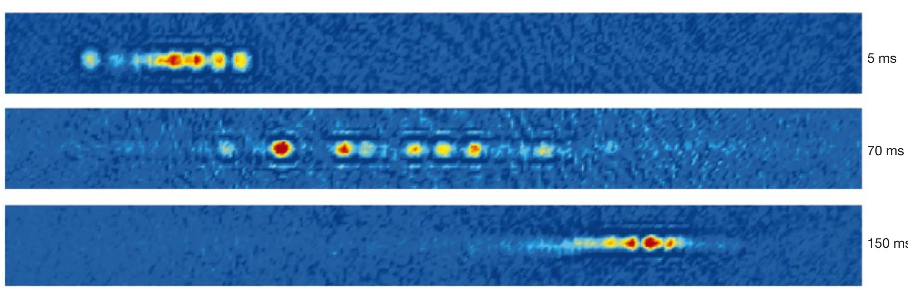

Figure 1.4: Soliton train as produced by Strecker *et al.* [17]. The group of solitons propagate without combining or dispersing.

In 2002 bright solitons were formed in two separate experiments. Khaykovich *et al.* [16] produced matter-wave bright solitons in an ultracold lithium-7 gas. They compared results of two systems with different scattering lengths as shown in Figure 1.3. The propagation of an ideal gas, where $g = 0$, results in the BEC dispersing. In the system with attractive interactions, the BEC propagated without dispersion over 1.1mm, giving the indication of a soliton.

Simultaneously at Rice University, Strecker *et al.* [17] formed matter-wave soliton trains. A group of bright solitons of lithium-7 atoms in a quasi-1D waveguide were observed to propagate without spreading for many oscillatory cycles, as shown in Figure 1.4. The solitons did not merge together due to the relative phase, which was set to be $\phi = \pi$.

In 2013 physicists at Durham University formed a Rubidium BEC containing a bright solitary matter-wave. Marchant *et al.* examined the reflection of the soliton from a Gaussian barrier contained within a harmonic trap [18]. They observed experimentally the effects the barrier had on the dynamics of the soliton and in Section 3.3 we recreate their results in a numerical model.

There is currently much theoretical interest in the stability of solitons in collisions and how these theories can be applied in physical systems [15]. A potential application for bright solitons in BECs is interferometry, a method for extracting information about forces. Experiments have previously relied on manipulating waves of light and precision in measurements was poor. The properties of bright solitary waves offer the opportunity for improving the precision. Interferometers are able to split the BEC and recombine it after a period. Differences in properties and phase give indication to the conditions of the separate paths which the split BEC takes. This technique of investigation is important in applications to astronomy, oceanography and fibre optics.

There are two main ways to model solitons theoretically. An analytical soliton solution to the nonlinear wave equation can be found and solved in very limited cases, e.g. for a stationary soliton, but we are interested in more dynamical systems. Since solitons do not experience dispersion, they can be modelled as particles in a much simpler system. Hamiltonian mechanics are a platform used for modelling the quantum mechanics of solitons numerically. Although this method neglects the internal excitations of solitons, it allows us to calculate soliton trajectories without having to solve the full nonlinear wave equation. Martin *et al.* [19] show that the classical particle dynamical model shows good agreement with the full solution of the wave equation. This classical particle model is what we develop further in this dissertation.

Chapter 2

Theory

2.1 Gross-Pitaevskii Equation

To a good approximation the dynamics of a BEC can be described by the Gross-Pitaevskii Equation [20, 21], the GPE, which is a specific form of the nonlinear Schrödinger equation. It is a classical wave equation which arises from an approximation to the Heisenberg equations of motion [22]. The Gross-Pitaevskii equation in three dimensions is

$$i\hbar\frac{\partial}{\partial t}\Psi(\mathbf{r},t) = \left(-\frac{\hbar^2}{2m}\nabla^2 + V(\mathbf{r}) + g_{3D}N|\Psi(\mathbf{r},t)|^2\right)\Psi(\mathbf{r},t), \tag{2.1}$$

where $\Psi(\mathbf{r},t)$ denotes the wave-function and $\hbar$ is the reduced Planck's constant. The mass of each particle is given by m, g_{3D} is the strength of interaction, N is the number of particles in the BEC and $V(\mathbf{r})$ is the trapping potential. The trapping potential is a magnetic field which holds the BEC in space. It can be varied in time and space to manipulate the BEC. For convenience the wave-function is normalised to one. The GPE is a valid description given that the condensate is macroscopically populated $N \gg 1$ and the temperature of the gas is sufficiently low that $T \ll T_C$ holds.

Time independent solutions of the GPE have the form

$$\Psi(\mathbf{r},t) = \psi(\mathbf{r})e^{-\frac{i\mu t}{\hbar}} \tag{2.2}$$

where $\psi(\mathbf{r})$ is time-independent and μ is the chemical potential (constant), the energy required to add or remove a particle from the system. Substituting this expression into Equation (2.1) gives the time-independent form of the GPE as

$$\mu\psi(\mathbf{r}) = \left(-\frac{\hbar^2}{2m}\nabla^2 + V(\mathbf{r}) + g_{3D}N|\psi(\mathbf{r})|^2\right)\psi(\mathbf{r}), \tag{2.3}$$

solutions to which describe the stationary states of the system.

2.1.1 Trapping Potentials

BECs are typically confined by harmonic potentials, or traps, which have the general form

$$V(\mathbf{r}) = \frac{m}{2}\left(\omega_x^2x^2 + \omega_y^2y^2 + \omega_z^2z^2\right), \tag{2.4}$$

where ω_x, ω_y and ω_z are trap frequencies in the direction of each spatial coordinate. By changing the appropriate value of ω it is possible to change the shape of the potential. These frequencies can be controlled experimentally, allowing effective manipulation of the potential, and therefore the BEC, as displayed in Figure 2.1.

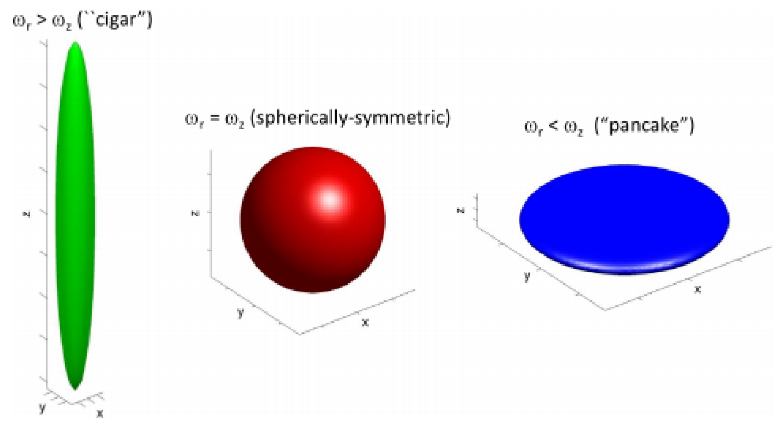

Figure 2.1: Example trapping potentials showing the effects of different restrictions [23].

2.1.2 Time-Independent Solutions

The time-independent GPE, given by Equation (2.3), can not, in general, be solved analytically when considering interactions and the harmonic trap. Considering a system with the absence of interactions, setting $g = 0$, the GPE becomes the Schrödinger equation as there is no longer the nonlinear term. The Schrödinger equation describes a single particle instead of a system of partcles. In the harmonic trap, the Gaussian is an exact solution which is given by

$$\psi(\mathbf{r}) = \frac{1}{\pi^{3/4} {l_r}^{3/2}} \exp\left(-\frac{r^2}{2{l_r}^2}\right) \tag{2.5}$$

where $l_r = \sqrt{\hbar/m\omega_r}$ and l_r denotes the width of the Gaussian [23]. It is valid for a spherically symmetric potential, i.e. $\omega_r = \omega_x = \omega_y = \omega_z$ as shown in centre of Figure 2.1.

2.1.3 Quasi-1D and Quasi-2D BECs

When the harmonic trapping is strong in one direction, the wave-function varies rapidly in that direction. This causes the Laplacian term in the GPE to become large. Considering the terms in the GPE, both the potential and Laplacian terms are large, and in comparison the remaining term, the nonlinear term, becomes small. Neglecting this term the GPE reduces to the Schrödinger equation, for which we expect a Gaussian solution as detailed above.

When the harmonic trapping is very strong in one (or more) directions, the wave-function in that direction approximates to the time-independent ground harmonic oscillator state, i.e. the Gaussian. The dynamics only occur in the more weakly trapped directions, and hence we can form systems with reduced dimensionality by adjusting the frequency parameters.

Restricting the harmonic potential in one direction is achieved by setting $\omega_x = \omega_y \ll \omega_z$. The difference in frequencies opens up the trap in two directions and squeezes in the other, producing the "pancake" (right in Figure 2.1) which is considered quasi-2D.

For a quasi-1D trap, the potential is restricted in two directions with $\omega_x = \omega_y \gg \omega_z$, producing the "cigar" (left in Figure 2.1). The high frequencies squeeze the trap radially and the condensate and trap can be considered to be in one dimension. We proceed by considering a quasi-1D system in x and so the potential $V(\mathbf{r})$ becomes $V(x) = m\omega_x^2 x^2/2$.

2.1.4 One-Dimensional Gross-Pitaevskii Equation

To produce one dimensional objects like solitons, the dynamical system should have the same dimensional properties. We can draw simpler conclusions more efficiently by reducing the three dimensional GPE to an equation with only one spatial coordinate [22]. To obtain the one-dimensional GPE analytically, we take this decomposition of the wave-function in the y and z directions,

$$\Psi(\mathbf{r},t) = \psi(x,t)\Phi(y)\Phi(z) \qquad \text{where} \qquad \Phi(\zeta) = \left(\frac{1}{\sigma^2\pi}\right)^{1/4} \exp\left(-\frac{\zeta^2}{2\sigma^2}\right). \tag{2.6}$$

The wave-function has a Gaussian form with $\sigma^2 = \hbar/m\omega_r$ [19] and we can integrate out in the y and z directions by applying the operator

$$\int_{-\infty}^{\infty}\int_{-\infty}^{\infty} \Phi^*(y)\Phi^*(z)dydz. \tag{2.7}$$

which "averages" the wave-function in the radial directions. Applying restrictions (as defined in Section 2.1.3) to the potential so that it is sufficiently tight in the y and z directions, the harmonic trap potential energy is effective only in the x direction. And so (2.1) becomes

$$i\hbar\frac{\partial}{\partial t}\psi(x,t) = \left(-\frac{\hbar^2}{2m}\frac{\partial^2}{\partial x^2} + \frac{m\omega_x^2 x^2}{2} + g_{1D}N|\psi(x,t)|^2 + \hbar\omega_r\right)\psi(x,t). \tag{2.8}$$

noting here how the derivatives are now only in x and the strength of interaction has changed to reflect the reduction in dimension.

The dimensionless form of the GPE allows us to find the simplest numerical form of the solution. Introducing the dimensionless variables

$$\begin{aligned} \widetilde{x} &= \frac{m|g_{1D}|N}{\hbar^2}x, & \widetilde{t} &= \frac{m|g_{1D}|^2N^2}{\hbar^3}t, \\ \widetilde{\omega} &= \frac{\hbar^3}{m|g_{1D}|^2N^2}\omega_x, & \widetilde{\psi}(\widetilde{x}) &= \frac{\hbar}{\sqrt{mg_{1D}N}}\Psi(x). \end{aligned} \tag{2.9}$$

Equation (2.8) becomes

$$i\frac{\partial}{\partial \widetilde{t}}\widetilde{\psi}(\widetilde{x},\widetilde{t}) = \left[-\frac{1}{2}\frac{\partial^2}{\partial \widetilde{x}^2} + \frac{1}{2}\widetilde{\omega}^2\widetilde{x}^2 - |\widetilde{\psi}(\widetilde{x},\widetilde{t})|^2\right]\widetilde{\psi}(\widetilde{x},\widetilde{t}). \tag{2.10}$$

Applying the same relations to the time-independent GPE, we obtain

$$\mu\widetilde{\psi}(\widetilde{x}) = \left[-\frac{1}{2}\frac{\partial^2}{\partial x^2} + \frac{1}{2}\widetilde{\omega}^2\widetilde{x}^2 - |\widetilde{\psi}(\widetilde{x})|^2\right]\widetilde{\psi}(\widetilde{x}). \tag{2.11}$$

Now that every variable is dimensionless we proceed using these quantities and can remove the 'tilde' notation. Considering a system in open space, with no potential ($\omega = 0$), we seek a solution of the dimensionless form $\psi(x,t) = \psi(x)e^{-i\mu t}$. We take the trial solution,

$$\psi\left(x\right) = A\,\mathrm{sech}\,\frac{x}{B} \qquad \text{which gives} \qquad \psi\left(x\right) = \sqrt{2|\mu|}\,\mathrm{sech}\left(\sqrt{2|\mu|}x\right). \tag{2.12}$$

The sech form of the solution demonstrates the wave is localised in nature. The solution is time-independent and there is no trapping along x and so the wave is held together by the attractive interactions only. Hence it is a soliton solution.

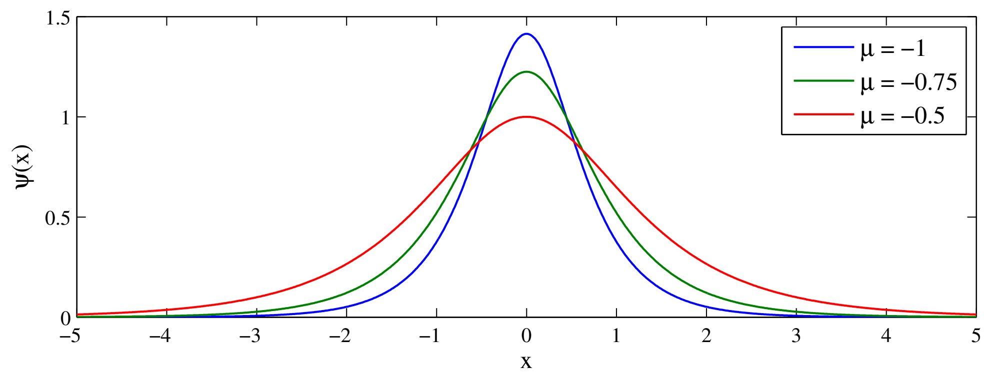

Figure 2.2: The exact soliton solution to the GPE for different values of μ.

2.1.5 The Effective Mass

Following methods used by Martin *et al.* in [19] the wave-function is normalised to one. The norm is given by

$$\mathcal{N} = \int_{-\infty}^{\infty} |\psi\left(x\right)|^2 dx = 4\eta \tag{2.13}$$

which is set such that $\mathcal{N} = 1$. So when considering a one soliton system, $\eta = 0.25$; for two solitons $\eta_1 = \eta_2 = 0.125$.

2.2 Hamiltonian Mechanics

To avoid solving the full GPE to calculate the trajectories of the soliton, we use Hamiltonian mechanics as a platform for modelling the motion numerically. The exact solution given by Equation (2.12) confirms the localised nature of the solitary wave solution such that we can model it as a particle. Hamiltonian mechanics allows us to derive equations of motion so we can consider the particle dynamics within various systems. This classical particle approximation has been shown to agree well with full numerical solutions of the GPE by Martin *et al.* [19].

The Hamiltonian describes the energies of the system; remaining constant, H is the sum of the kinetic and potential energies. When considering a system with one soliton, the Hamiltonian is given by,

$$H = \frac{p^2}{2\eta} + \frac{1}{2}\eta\omega^2 q^2. \tag{2.14}$$

The Hamiltonian is given as a function of position q and momentum p; this is reflected in how the kinetic and potential energies are expressed. Equation (2.14) is appropriate for a simple system which models the particle dynamics of a single soliton in a harmonic trap. The first term refers to the kinetic energy, the second term the potential energy. This is the relevant potential energy for a harmonic trap with frequency ω. There is an individual Hamiltonian for each respective system of solitons.

Hamilton's equations are applied to the Hamiltonian and we obtain equations of motion. The equations describe the motion of the particle as a coupled system of two first order differential equations,

$$\frac{dq}{dt} = \frac{\partial H}{\partial p} \quad \text{and} \quad \frac{dp}{dt} = -\frac{\partial H}{\partial q}. \tag{2.15}$$

They can be considered as giving, at each point (q, p) of phase space, the velocity vector $(\dot{q}, \dot{p})$ used for building all the trajectories $(q(t), p(t))$ [24]. Upon solving these ODEs, we can obtain values for position and momentum of the particle at each time step. Typically we solve the ODEs numerically using MATLAB.

Chapter 3

Single Soliton Model

As motivation for our modelling, we aim to recreate an experiment recently completed by Marchant *et al.* [18]. The experiment mapped the dynamics of a soliton contained in a harmonic potential with a barrier in the trap wall. We explore to what extent these results can be found numerically. In this chapter we investigate the dynamics of the particle for different systems, increasing the complexity of the potential each time.

3.1 Dynamics in an Open Space

Consider a system with no trapping potential; a soliton is moving in a completely flat open space. Without any potential, the Hamiltonian is given by $H = p^2/2\eta$ which is independent of time. It follows that the motion of the particle in this system is trivial as it would remain constant and not change in direction or speed at all as time propagates.

3.2 Dynamics in a Harmonic Trap

For a non-trivial system we introduce a harmonic trapping potential as described in Section 2.1.3. For our one dimensional system our potential is given by

$$V(q) = \frac{1}{2}\eta\omega^2 q^2 \tag{3.1}$$

where η is the effective mass, ω is the trap frequency and q is the position of the particle. For this system we obtain the Hamiltonian,

$$H = \frac{p^2}{2\eta} + \frac{\eta\omega^2 q^2}{2}, \tag{3.2}$$

which we solve to obtain Hamilton's Equations:

$$\frac{dp}{dt} = -\eta\omega^2 q^2 \quad \text{and} \quad \frac{dq}{dt} = \frac{p}{\eta}. \tag{3.3}$$

These coupled ordinary differential equations can be solved analytically. Combining them we obtain this second order ODE, $\ddot{q} + \omega^2 q = 0$, which describes the motion of the particle. The solution is given by

$$q(t) = A\sin\omega t + B\cos\omega t \tag{3.4}$$

where A and B are constants to be determined by initial conditions. The system is an example of a simple harmonic oscillator; the trajectory of motion for the soliton is sinusoidal about the origin of the trap.

Having obtained a solution for the system analytically, we simulate these results numerically using MATLAB to validate the code and accuracy of the ODE solver. As we are following the experiment which includes the barrier, we keep the trap frequency consistent with that given by Marchant *et al.* [18]. Taking the experimental value, we apply the dimensionless variables given in Equation (2.9) to convert into dimensionless values suitable for our model. We set the trap frequency as specified by [18], $\omega = 0.03$, and the effective mass $\eta = 0.25$.

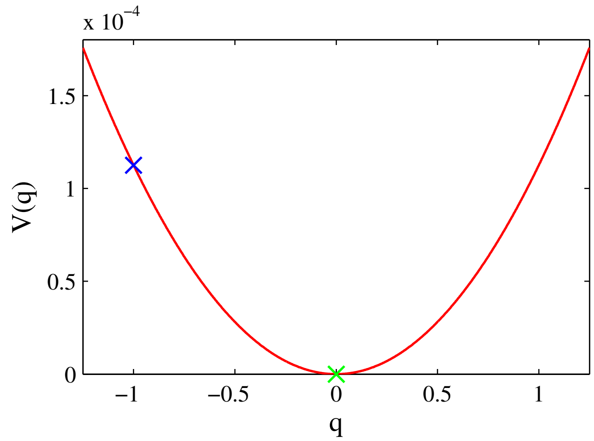

Figure 3.1: Plot of harmonic trapping potential. The green cross represents the initial position of case 1, and the blue cross for case 2.

We consider one soliton in two cases with different initial conditions as shown by the crosses in Figure 3.1;

1. Soliton placed in the centre of the trap, with momentum: $q(0) = 0$, $p(0) = 0.0075$ (green);
2. Soliton placed up the trap wall, without momentum: $q(0) = -1$, $p(0) = 0$ (blue).

We solve Hamilton's Equations for each of these cases as shown in Figure 3.2.

Case 1: $q(0) = 0$**,** $p(0) = 0.0075$

The simulation for the first set of initial conditions is represented by the blue line in Figure 3.2. We consider the motion of the soliton as it is placed at the origin in the centre of the harmonic trap. The soliton begins with a small momentum and travels up the wall of the trap. As it moves up, the soliton loses kinetic energy but gains potential energy. At $t \approx 100$ the soliton reaches its maximum height up the trap wall and is stationary. The soliton then begins to accelerate back down the trap wall to the centre of the trap, losing potential energy and gaining kinetic energy. As it travels up the opposite side the soliton decelerates again. This motion continues in the form of an oscillation with a sinusoidal shape. We obtain the exact solution for this trajectory; recalling Equation (3.4) we apply our initial conditions and calculate for case 1 $q(t) = \sin \omega t$. This analytical solution follows the blue trajectory in Figure 3.2 exactly.

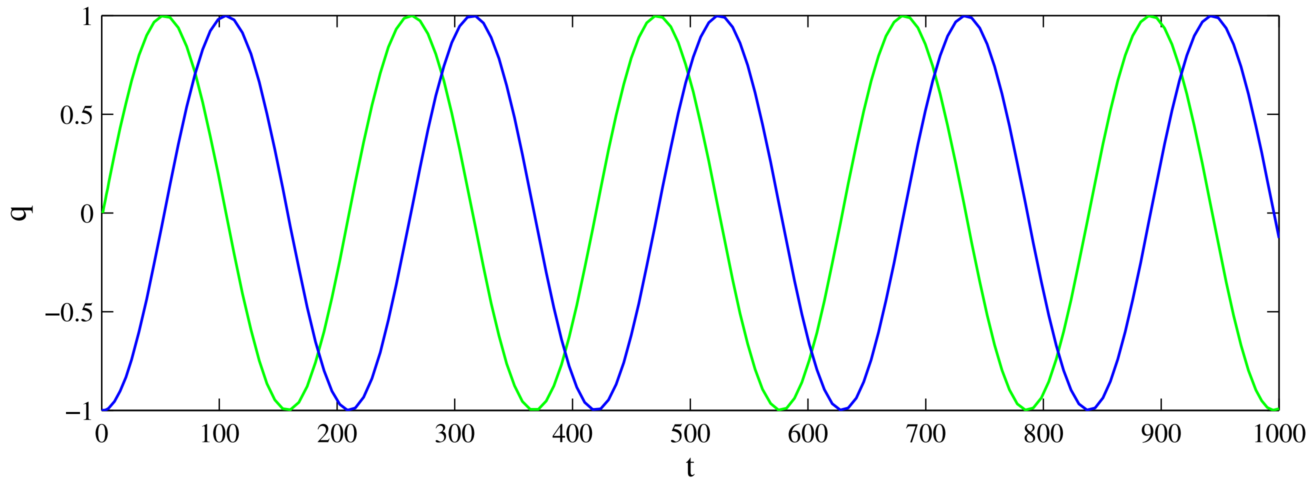

Figure 3.2: A position - time plot of a single soliton in a symmetric harmonic trap for differing sets of initial conditions. Following conditions set by Marchant *et al.* [18] $\omega = 0.03$.

Case 2: $q(0) = -1$, $p(0) = 0$

The green line in Figure 3.2 depicts the simulation for the second set of initial conditions. We consider the motion of the soliton as it is displaced from the origin; placed at position $q = -1$ the soliton begins the its trajectory up the trap wall with potential energy and no kinetic energy. The soliton travels down the trap wall, accelerating it gains kinetic energy and losing potential energy. The soliton passes through the origin and starts decelerating as it travels up the opposite trap wall. At $t \approx 230$ the soliton reaches its maximum height and is stationary. It then travels back down the trap wall and the oscillation forms. As before we compare with the analytical solution. Having applied this set of initial conditions we obtain that for case 2 $q(t) = -\cos \omega t$.

As a check, we calculate the overall energy of the system at each time interval. We require the energy level to remain constant however there is a slight decrease in energy over time. The relative error is 0.0017 therefore we can conclude that there is no significant loss of energy from the system. It is concluded that these errors originate from a relative tolerance level built into the ODE45 solver in MATLAB. Decreasing the tolerance improves the results.

3.3 Dynamics in a Harmonic Trap with a Barrier

3.3.1 The Experimental Potential

The introduction of the barrier into the trapping potential complicates the system and makes our results more interesting. To include the Gaussian barrier in the trap we add the barrier term to expression for the potential.

$$V(q) = \frac{m\omega^2 q^2}{2} + V_0 \exp\left[-\frac{(q - q_0)^2}{w^2}\right] \tag{3.5}$$

where V_0 is the barrier height, w the barrier width and q_0 is the barrier position. These parameters allow us to adjust the shape and size of the barrier, and therefore adjust the effects the barrier can have on the motion of the soliton. The conditions chosen ensure the barrier is much wider than the solitary wave and so the wave behaves classically. As before we use the dimensionless variables given in Equation (2.9) to convert the experimental values given by Marchant *et al.* [18] into dimensionless values, suitable for our model. In Figure 3.3 the Gaussian barrier can be seen; the black line represents the shape of the transformed potential; the red dotted line shows the original potential from Section 3.2; the blue cross is the initial starting point of the soliton in the system. This initial position is clearly chosen to be above the barrier on the trap wall, i.e. $|q(0)| > |q_0|$.

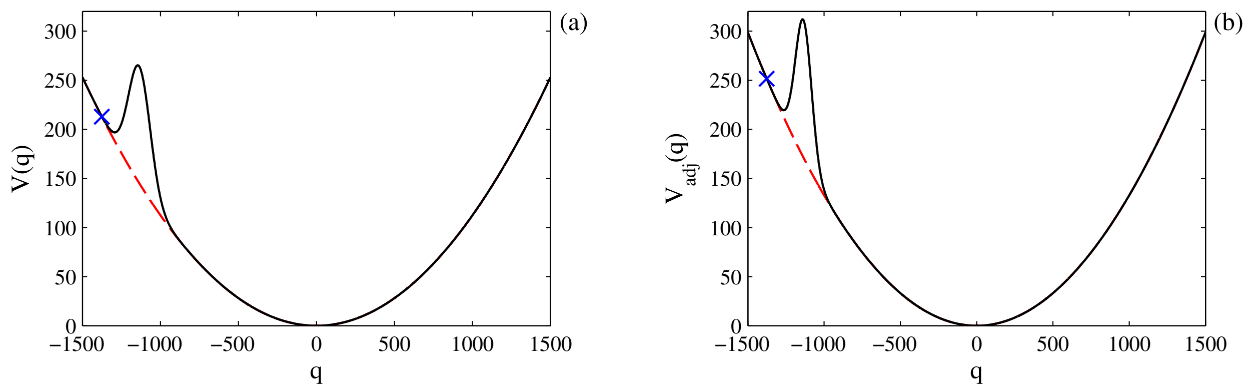

Figure 3.3: Plot of the harmonic trap with barrier for (a) original model with conditions based on those used by [18]: $\omega = 0.03,\ V_0 = 119,\ w = 98,\ q_0 = -1135$; (b) adjusted model with conditions: $\omega = 0.0326,\ V_0 = 140,\ w = 75,\ q_0 = -1135$.

3.3.2 Comparison to Experimental Dynamics

Having set the conditions we proceed with the theoretical simulation. The soliton is released from its initial position with zero momentum and the motion is mapped in Figure 3.4. Throughout the simulation, we compare the barrier results (in black) with the experimental model (in red) where the trap is without a barrier. The blue and green dots signify data obtained from the original study. Figure 3.4 is a plot showing the distance travelled from the initial position over time. The gradient of the lines represent the velocity of the soliton.

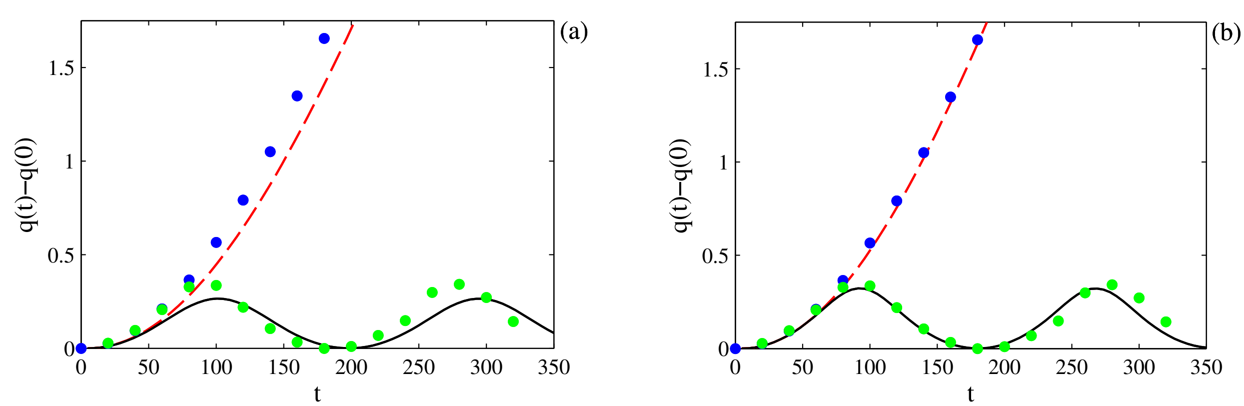

Figure 3.4: Plot of the distance travelled over time for (a) original model and (b) adjusted model with initial conditions $q(0) = -1376,\ p(0) = 0$.

We consider the motion of the soliton as it interacts with the barrier depicted by the black line. The soliton is released from rest and travels down the side of the trap; it decelerates as it moves up the barrier wall and accelerate as it moves back down. The soliton has been reflected by the barrier; it returns to its initial position and an oscillation is instigated (c.f. Section 3.2 Case 2). It is as if the soliton is held in a small version of the harmonic trapping potential. The red dotted line represents the trajectory in a system without the barrier. Without the barrier in the trap, the soliton is not reflected and continues towards the centre of the trap.

The data from the experimental study is overlaid and we see that it captures the overall qualitative behaviour of the dynamics but there is a slight mismatch. We adjust the model parameters to find a theoretical simulation which is closer to the data. We make adjustments to the parameters; increasing the barrier height and decreasing the width makes the walls of the barrier steeper which, in turn, decreases the period of the oscillation. A slight increase in the trap frequency similarly makes the walls of the trap steeper which evens out the oscillation. See the adjusted potential in Figure 3.3(b) and the effects these changes had on the adjusted model in Figure 3.4(b). Now that the model follows the data much closer, we assume these model parameters and proceed.

3.3.3 The Effect of Varying the Barrier Height

We consider how the dynamics change as we decrease the barrier height. It is interesting to explore at what height the soliton is no longer reflected but is transmitted over the barrier. Having already examined the results for $V_0 = 0$ and $V_0 = 140$ we consider four barrier heights in between these values which best show the changes in dynamics as the height of the barrier is altered.

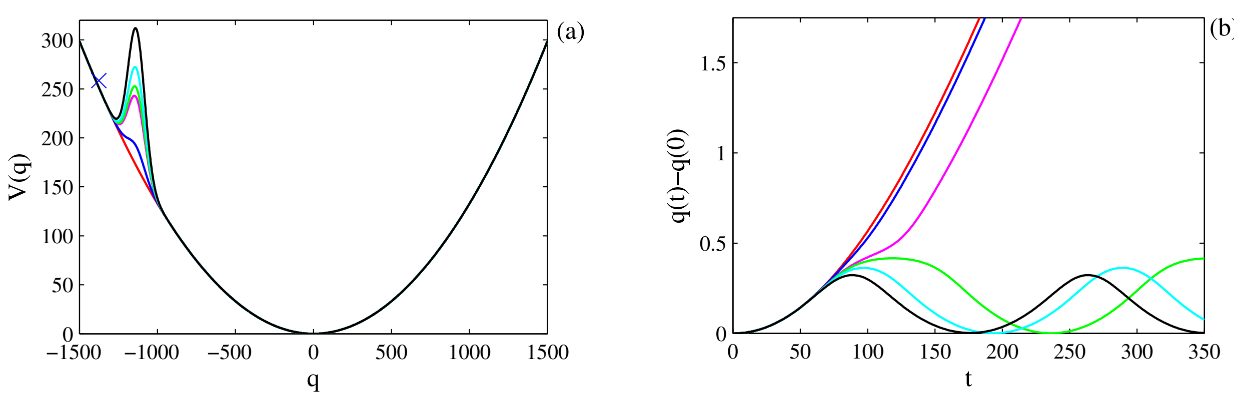

Figure 3.5: Plot of harmonic potential, (a), and plot of distance travelled over time, (b), with varying barrier heights. The specific heights for the respective coloured lines are $V_0 = 0$, $V_0 = 20$, $V_0 = 70$, $V_0 = 80$, $V_0 = 100$ and $V_0 = 140$.

In Figure 3.5 we are able to see the effect the barrier height has on the results. Similarly to Figures 3.5(b) and 3.4(b), it shows the distance travelled from the initial position over time. We consider the case when $V_0 = 20$; represented by the blue line, we see that at $t \approx 80$ the path of the soliton differs slightly from the original model when there is a small deceleration as the soliton passes over the barrier. In the next case when $V_0 = 70$, shown in magenta, the soliton has similar dynamics. The deceleration lasts longer as the barrier is higher and this is reflected in the plot. We obtain very different results for $V_0 = 80$ (shown in green), despite the small increase in barrier height. The small increase in barrier height is enough to cause a reflection from the barrier and we see an oscillation occur. This oscillation has a larger period as the soliton spends more time on the barrier. Finally we consider the cyan line when $V_0 = 100$, which shows the path of the soliton almost meeting the black line. From this analysis we see the most interesting results when the barrier height is between 70 and 80.

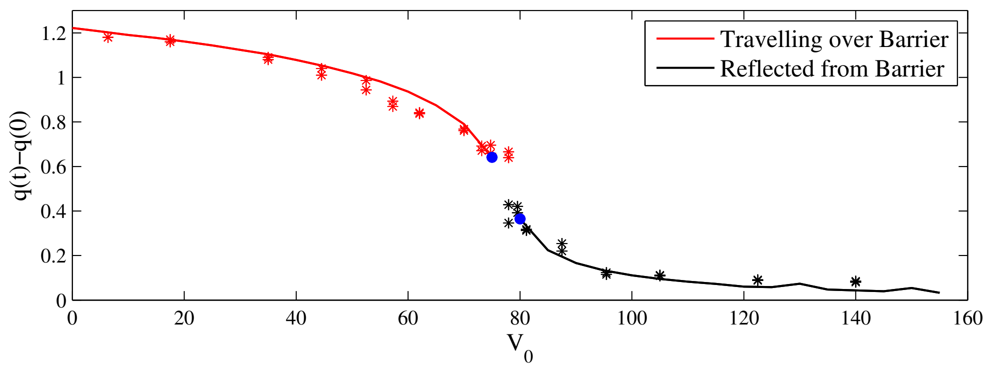

Figure 3.6: Plot of distance travelled against barrier height which demonstrates the heights of barrier for which the soliton is transmitted or reflected.

A different representation of these conclusions is given in Figure 3.6. Here we consider the distance the soliton is able to travel within 150ms plotted against varying barrier heights. The red line represents the cases when the soliton travels over the barrier, with the barrier height small. The black line shows the cases when the soliton is reflected. This plot demonstrates the overall effect the barrier height has on the distance travelled; for small barriers, the soliton travels further; for high barriers, the distance travelled from the initial point is much smaller. The blue dots show the points which are most crucial for the model. Between the blue dots is a critical barrier height which divides systems where the particles travel over the barrier from systems where the particles are reflected.

In this chapter we considered a system for a single soliton. Solving Hamilton's equations analytically gave validation for the results obtained from simulating the system in MATLAB. Extending the model, we included a barrier in the harmonic trap and compared the simulated values to experimental results. We made adjustments to the model to improve agreement and explored the effect of varying the height of the barrier. A final comparison with experimental results in Figure 3.6 is made; the model agrees with the data very well and this confirms the validity of the model.

Chapter 4

Two-Soliton Dynamics: The Interaction Potential

This section examines systems of two solitons. Each soliton has position q_i, momentum p_i and mass η_i. To consider this system, we adapt our model as in multiple soliton systems there are other energies to be considered. As we saw Section 1.2.3, the s-wave scattering controls the strength of the interaction which holds the BEC together. When the tails of the soliton wave-packets overlap, they interact with each other. We explore how this interaction affects the dynamics of the solitons in the system.

The interaction potential reflects the attractive or repulsive nature of the solitons. For two solitons it is defined as

$$V_{Int}\left(q_1 - q_2\right) = E\left(q_1 - q_2\right) - E\left(q_1\right) - E\left(q_2\right) \tag{4.1}$$

where $E\left(q_1, q_2\right)$ is the energy of a two-soliton system, and $E\left(q_i\right)$ is the energy of the one-soliton system. When the solitons are far apart, there is no interaction between the solitons and the energy of the two-soliton system is equal to the separate one-soliton systems, and $V_{Int} = 0$. When the solitons are in close proximity, the interaction is felt, $E\left(q_1, q_2\right) < E\left(q_1\right) + E\left(q_2\right)$ and the interaction potential is negative. Itl can be derived [25] as

$$V_{Int}\left(q_i - q_j\right) = -2\eta_i\eta_j\left(\eta_i + \eta_j\right)\operatorname{sech}^2\left[\frac{2\eta_i\eta_j}{\eta_i + \eta_j}\left(q_i - q_j\right)\right] \tag{4.2}$$

where $q_i - q_j$ is the relative separation of each pair of solitons. For a system with several solitons, there is an interaction energy for each soliton pair and it is crucial to include them all when calculating the energy of the system.

The negative sech^2 form of the potential causes the solitons to behave as if they have entered a 'bowl-like' potential. Only effective when they are in the region of one another, we expect an acceleration as they approach one another, and a deceleration as they separate. When the separation is close to zero the magnitude of V_{Int} is at its greatest.

The Hamiltonian

We adjust the Hamiltonian, Equation (2.14), to include the interaction energy for a two-soliton system and obtain

$$H = \frac{p_1^2}{2\eta} + \frac{p_2^2}{2\eta} + \frac{1}{2}\eta\omega^2 q_1^2 + \frac{1}{2}\eta\omega^2 q_2^2 - 2\eta_1\eta_2\left(\eta_1 + \eta_2\right)\operatorname{sech}^2\left[\frac{2\eta_1\eta_2}{\eta_1 + \eta_2}\left(q_1 - q_2\right)\right] \tag{4.3}$$

As before, this equation includes terms for the kinetic energies and the potential energies for each soliton. The potential energies include the interaction and harmonic trap terms; for cases without a trap, we set $\omega = 0$.

From this we can obtain Hamilton's equations; for a two-soliton system there are two equations per soliton. For the first soliton,

$$\begin{aligned} \frac{dq_1}{dt} &= \frac{\partial H}{\partial p_1} \qquad \text{and} \qquad & \frac{dp_1}{dt} &= -\frac{\partial H}{\partial q_1} \\ &= \frac{p_1}{\eta_1} & &= -\eta_1 \omega^2 q_1 - \frac{\partial V_{Int}}{\partial q_1}, \end{aligned} \tag{4.4}$$

and similarly for the second soliton,

$$\begin{aligned} \frac{dq_2}{dt} &= \frac{\partial H}{\partial p_2} \qquad \text{and} \qquad & \frac{dp_2}{dt} &= -\frac{\partial H}{\partial q_2} \\ &= \frac{p_2}{\eta_2} & &= -\eta_2 \omega^2 q_2 - \frac{\partial V_{Int}}{\partial q_2}, \end{aligned} \tag{4.5}$$

where

$$\begin{aligned} \frac{\partial V_{Int}}{\partial q_1} &= 8\eta_1^2\eta_2^2 \tanh\left[\frac{2\eta_1\eta_2}{\eta_1+\eta_2}(q_1-q_2)\right]\operatorname{sech}^2\left[\frac{2\eta_1\eta_2}{\eta_1+\eta_2}(q_1-q_2)\right], \\ \frac{\partial V_{Int}}{\partial q_2} &= -8\eta_1^2\eta_2^2 \tanh\left[\frac{2\eta_1\eta_2}{\eta_1+\eta_2}(q_1-q_2)\right]\operatorname{sech}^2\left[\frac{2\eta_1\eta_2}{\eta_1+\eta_2}(q_1-q_2)\right]. \end{aligned}$$

In this report we only consider solitons of equal mass so we set $\eta_1 = \eta_2 = \eta$. Therefore we can simplify the interaction potential to become

$$V_{Int}(q_1-q_2) = -4\eta^4 \operatorname{sech}^2[\eta(q_1-q_2)] \tag{4.6}$$

and thus Hamilton's equations, (4.4) and (4.5), become

$$\frac{dq_1}{dt} = \frac{p_1}{\eta} \qquad \text{and} \qquad \frac{dp_1}{dt} = -\eta\omega^2 q_1 - 8\eta^4 \tanh\eta(q_1-q_2)\operatorname{sech}^2\eta(q_1-q_2), \tag{4.7}$$

$$\frac{dq_2}{dt} = \frac{p_2}{\eta} \qquad \text{and} \qquad \frac{dp_2}{dt} = -\eta\omega^2 q_2 + 8\eta^4 \tanh\eta(q_1-q_2)\operatorname{sech}^2\eta(q_1-q_2). \tag{4.8}$$

Having derived this system of four ordinary differential equations, we proceed by solving them numerically in MATLAB. This results in simulated values which can be used to describe the dynamics of each particle in the system. We follow the work done by Martin *et al.* and use conditions of the system as set in [19]. The trap frequency is given as $\omega = 0.014$ and the effective mass of each soliton as $\eta_1 = \eta_2 = 0.125$.

4.1 Short Term Dynamics

In the model, we specify the initial conditions such that soliton 1 has $q_1(0) > 0$, $p_1(0) < 0$, while soliton 2 has $q_2(0) < 0$, $p_2(0) > 0$. This ensures that over a given time, the solitons will collide and interact. Altering the speeds allows us to control the nature of the interaction; when the solitons are moving slower, the interaction lasts longer, and therefore has more of an effect, whereas for fast moving solitons the interaction is negligible.

We consider three specific cases in the model to observe the full effects of the interaction energy, as shown in Figure 4.1;

(a) Both solitons moving without a harmonic trap;

(b) Soliton 1 is stationary; soliton 2 travels towards it without a harmonic trap;

(c) Both solitons moving symmetrically in a simple harmonic trap.

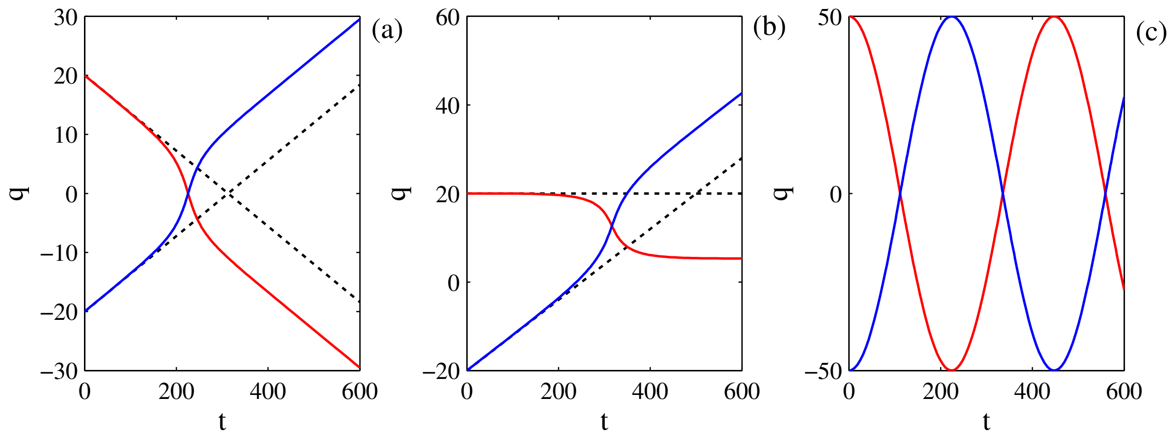

Figure 4.1: Position - time plots for soliton 1 and soliton 2 with initial conditions (a) $q_1(0) = 20,\ p_1(0) = -0.008,\ q_2(0) = -20,\ p_2(0) = 0.008$; (b) $q_1(0) = 20,\ p_1(0) = 0,\ q_2(0) = -20,\ p_2(0) = 0.01$; (c) $q_1(0) = 50,\ p_1(0) = 0,\ q_2(0) = -50,\ p_2(0) = 0$.

Figure 4.1 represents the paths of the solitons in the system; at every time step we can see their individual positions and velocities and also see how they interact. In each case, after the interaction both solitons return to their initial velocities before the collision. This retention of form and speed is a key property of solitons as defined in Section 1.1.

In Figure 4.1(a), the solitons approach each other, collide, interact and continue with their original velocities. During the interaction there is a shift in position for both soliton; we call this the "phase shift" and it is the only indication that any interaction has occurred. The interaction is most noticable in the Figure 4.1(b), with only soliton 2 initially moving. As soliton 2 approaches, the interaction causes soliton 1 to start moving. As with the first case, it then returns to it's initial velocity, at rest, but the phase shift is very clear. Case (c) consider the solitons in a harmonic trap. Despite both solitons starting from rest, they have high velocities when they collide at the bottom of the trap. No phase shift is obvious and so we are unable to observe any interaction that might have occurred.

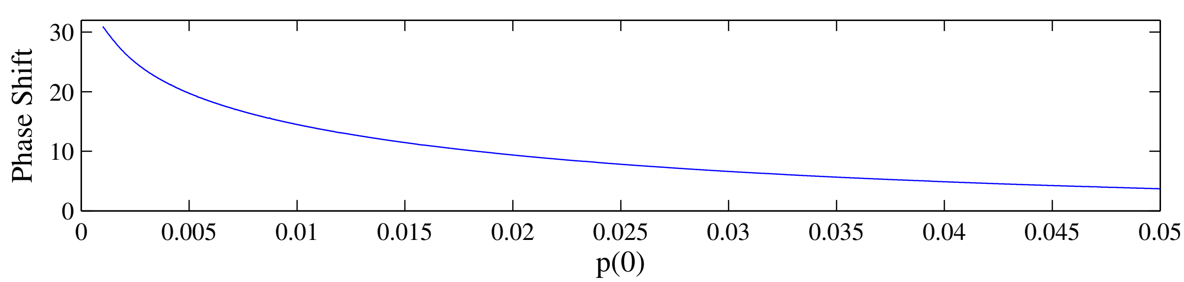

Figure 4.2: Plot examining the effect of initial momentum on phase shift for a system with one soliton approaching and interacting with a stationary soliton.

The dotted lines in Figure 4.1 demonstrate the trajectories of the solitons if there was no interaction, highlights the shift in position. It has been discussed how changing the initial speeds of the solitons can control the length of the interaction. Figure 4.2 examines how these conditions affect the size of the phase shift. It shows a system similar to Figure 4.1(b); one soliton approaches the other stationary one, with initial momenta ranging $0-0.05$. As expected, the faster the soliton moves, the shorter the length of interaction and the phase shift is smaller, as shown on the plot.

4.2 Longer Term Dynamics

We wish to examine the effect of multiple collisions and achieve this by only considering cases in the harmonic trap and extending the timescale. The initial conditions are specified such that they are not equal; soliton 1 is released from rest up the trap wall and soliton 2 is stationary at the bottom of the trap. We consider three cases with soliton 1 released from various heights to understand the dynamics. The heights are chosen to effect the dominance of the interaction potential.

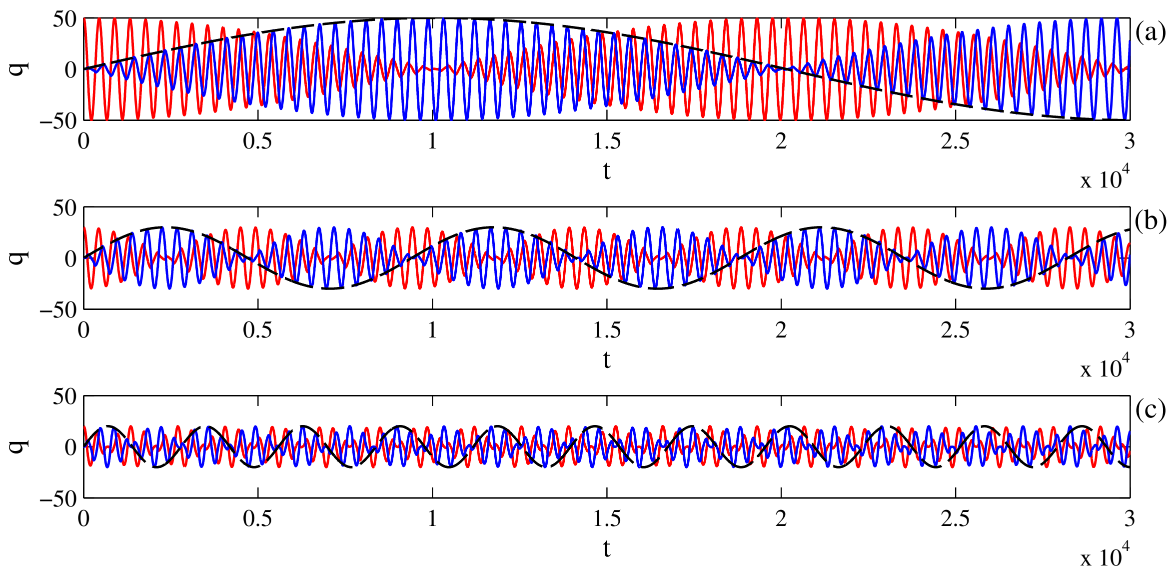

Figure 4.3: Position - time plots for soliton 1 and soliton 2 with initial conditions $q_2(0) = p_1(0) = p_2(0) = 0$ and (a) $q_1(0) = 50$, (b) $q_1(0) = 30$, (c) $q_1(0) = 20$. The black dashed lines in indicates the sinusoidal form of the oscillations.

Figure 4.3 describes the trajectories in each case. Every case successfully causes sufficient shift in the position of soliton 2 such that an oscillation in the trap is established. The time taken to achieve this varies based on the initial separation. In case (a) soliton 2 reaches its largest oscillation at $t \approx 1 \times 10^4$, for (b) this happens at $t \approx 0.25 \times 10^4$ and for (c) even earlier at $t \approx 0.1 \times 10^4$. A greater initial separation causes a higher difference in velocities when the solitons meet; the effect of the interaction is not as great and the oscillation takes longer to form.

The uneven initial conditions cause an energy transfer between the solitons. At $t = 0$ soliton 2 has no kinetic or potential energy and soliton 1 initially has high potential energy. As the propagation starts and the solitons interact the situation reverses; at $t = (1, 0.25, 0.1) \times 10^4$ for each respective case soliton 1 has almost zero energy and soliton 2 is at the highest positions of the trap with high potential energy. This repeats with the oscillation and there is a periodic transfer of energy between the solitons. This only occurs in cases with unequal initial conditions. In systems with symmetric initial positions (see Figure 4.1(c)) the oscillations are constant and there is no transfer of energy since when the solitons collide and interact their energy levels are the same. In a system with unequal initial conditions but without the interaction potential, there is no energy transfer and so soliton 2 remains stationary, despite the collision. The interaction potential is crucial for the continuous exchange of energy between solitons. It can generate systems with perpetual transfer of energy which might have useful real life applications in superconductivity.

4.3 Frequencies

The simulations are run for an extended time and it is observed that the trajectories of the solitons repeat, as is suggested in Figure 4.3(a). We notice oscillations take a sinusoidal form, particularly clear in (b), which are highlighted by the black dashed lines in each case. The period of the sinusoidal profile varies depending on the initial separation. When the solitons start further apart, in (a), the profile has a longer period compared to (c), when the initial separation is smaller and the period is shorter. This is due to the different frequencies found in the system which are effective for different initial separations. We investigate the form of these oscillations further and calculate the periods and frequencies as the initial conditions for the model changes. The sinusoidal profile and changes in amplitude of the oscillations is analogous to beats of sound waves. We investigate the frequencies of the system and look for a beat frequency to describe the sinusoidal shape.

We use various methods to determine the frequencies in the system. In MATLAB, the Discrete (Fast) Fourier Transform function produces a periodogram which picks out frequencies observed in the simulation. The trap frequency is clearly evident on the periodogram (Figure 4.4(a)) so we investigate the origins of other frequencies.

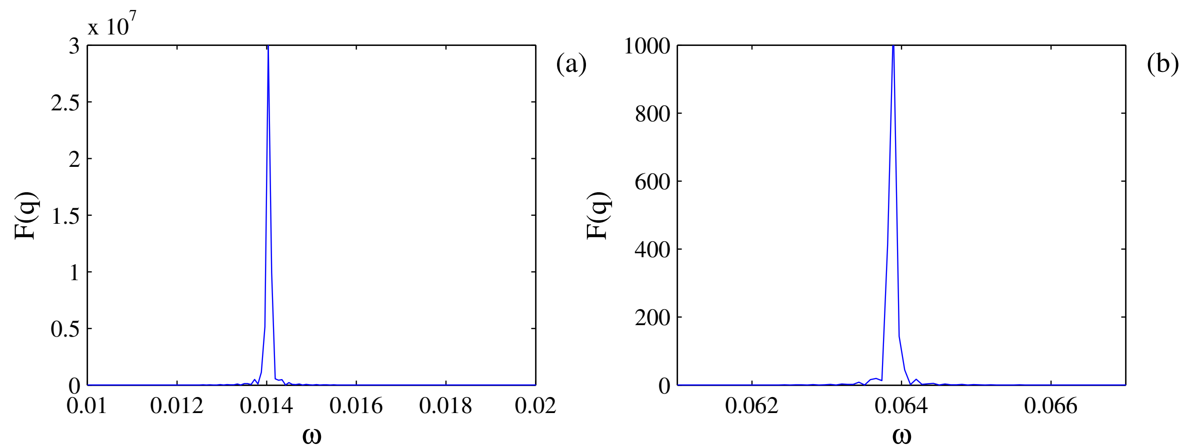

Figure 4.4: Periodograms showing frequencies of the interaction potential two-soliton system; (a) Fourier transform of the separation of two solitons with initial conditions $q_1(0) = 100,\ q_2(0) = p_1(0) = p_2(0) = 0$, similar to those in Figure 4.3, extracting $\omega \approx 0.014$; (b) Fourier transform of the separation of two solitons with symmetric initial conditions $q_1(0) = -0.3,\ q_2(0) = 0.3,\ p_1(0) = p_2(0) = 0$, extracting $\omega \approx 0.064$.

Earlier we discussed how the solitons are affected by the negative sech^2 form of the interaction energy. When the solitons are sufficiently close, the particles oscillate within the interaction potential with a frequency we refer to as the interaction frequency. We identify this frequency by taking a Taylor expansion of the interaction potential about the origin, to order $(q_1 - q_2)^2$, and obtain

$$V_{Int} \approx -4\eta^3 \left[1 - \eta^2 (q_1 - q_2)^2\right] \tag{4.9}$$

which we have shown as a decent approximation in Figure 4.5.

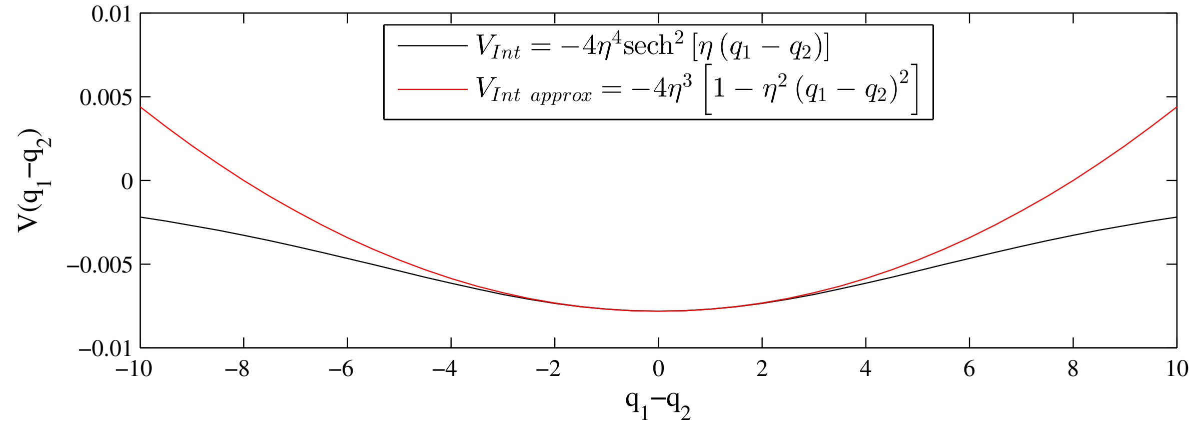

Figure 4.5: Comparison with Taylor series expansion for interaction potential.

To identify the interaction frequency, we compare like terms in the Taylor expansion with the expression for the harmonic trap potential. Comparing the magnitudes of the quadratic terms we obtain

$$\begin{aligned} 4\eta^5 (q_1 - q_2)^2 &= \frac{1}{4}\eta\omega_{int}^2 (q_1 - q_2)^2 \\ \implies \omega_{int} &\approx 0.0625. \end{aligned}$$

Combining the harmonic trap and interaction frequencies, the potential takes the form $V(q) = (\omega_{trap}^2 + \omega_{int}^2)q^2/2$. So we can obtain the combined frequency as given by

$$\begin{aligned} \omega_{comb} &= \sqrt{\omega_{trap}^2 + \omega_{int}^2} \\ &= \sqrt{0.014^2 + 0.0625^2} \\ \implies \omega_{comb} &\approx 0.064. \end{aligned}$$

This frequency is relevant for when the solitons have small separation and their motion is affected by both the trap and interaction frequencies. It is observed in Figure 4.4(b) in a system with these conditions.

4.3.1 Separation

As we saw in Figure 4.3, the initial separation determines the period of the sinusoidal profile of oscillations and so reflects the relative effect of the harmonic trap and interaction potential. We vary the initial separation from 0 to 100 in a symmetric system, and explore to what extent each potential energy is effective. For each system the period and angular frequency of oscillations are calculated by a function written in MATLAB. These values are determined based on the number

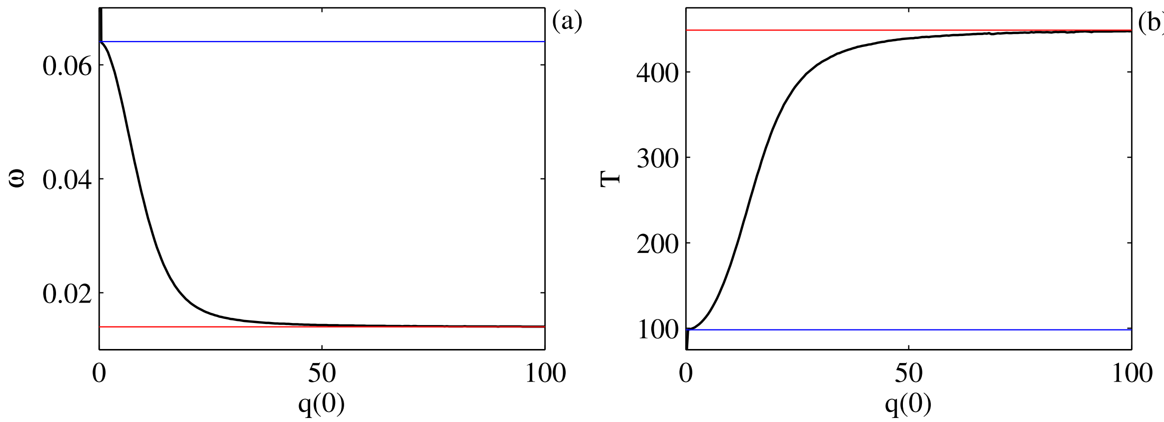

Figure 4.6: Examining the effect of initial separation on overall frequency (a) and period (b) of the system. Blue lines indicate the (a) $\omega_{comb} = 0.064$ and (b) $T = 98.2$; red line indicates (a) $\omega_{trap} = 0.014$ and (b) $T = 448.8$.

of times the trajectory crosses the origin. Due to the discrete nature of the iterations a degree of inaccuracy is expected, though minimised by the low relative tolerance in ODE45.

In Figure 4.6 we observe that the closer the solitons are together, the more they feel each others effect through the interaction potential (blue), which is consistent with Figure 4.3(c) when the period of oscillations is short. When the solitons start further apart, the more they feel the effect of the trap (red) and the longer the period (see Figure 4.3(a)). When the solitons start close together, very little time is spent propagating in the trap without the effects of the interaction and the opposite is true for when the solitons have large initial separation.

There is no indication of a beat frequency in the Fourier transform, nor are there any indications of additional forces felt in the separation simulation, so we are not able to explain the origin of the sinusoidal shape of the oscillations in the long-term dynamics.

4.4 Poincaré Sections

From the conclusions drawn from the modelling, we know that whilst the dynamics of the system are complicated there is a degree of recurrence within the results themselves. To analyse the complicated dynamics we seek a method of representing these results in a form which is easier to interpret. The phase space is three dimensional; there are four coordinates, q_1, p_1, q_2, p_2, but for a system with energy conserved, one of these can be eliminated [26]. A Poincaré section is used to decrease the number of dimensions of a phase space by one dimension. We introduce a surface of a section in phase space and, instead of studying a complete trajectory, we monitor only the points of intersection with this surface [27]. The Poincaré section shows points representing the intersection of an orbit with a plane. These points produce contours reflecting the region which is accessible a particular system. The section is not dependent on time; it is a representation of all the possible values for one soliton, with fixed conditions for the other. Introducing these restrictions on the data allows us to present the system in two dimensions.

To define the intersections we choose the plane to be $q_2 = 0$. When this condition occurs, soliton 2 can have positive or negative momentum. We choose $p_2 < 0$ for a unique definition of the Poincaré section. Applying these conditions, we compare the momentum and position of soliton 1 with the centre-of-mass energy.

4.4.1 Center-of-Mass Coordinates

For simplification when considering the separation of the solitons in the system, it is useful to introduce the relations [19]

$$Q = \frac{\eta_1 q_1 + \eta_2 q_2}{\eta_1 + \eta_2}, \qquad P = p_1 + p_2,$$
$$q = q_1 - q_2, \qquad p = \frac{\eta_2 p_1 - \eta_1 p_2}{\eta_1 + \eta_2}.$$

where Q is the center-of-mass position and q is the relative separation; P is the momentum canonically conjugate to Q and p is the momentum conjugate to q. In our simulations, the solitons are always of equal mass, so the center-of-mass relations become

$$Q = \frac{1}{2}\left(q_1 + q_2\right), \qquad P = p_1 + p_2,$$
$$q = q_1 - q_2, \qquad p = \frac{1}{2}\left(p_1 - p_2\right).$$

We make these substitutions and transform our expression for the Hamiltonian as given by Equation (4.3) to become

$$H = \frac{P^2}{4\eta} + \frac{p^2}{\eta} + \frac{\omega^2 \eta q^2}{4} + \omega^2 \eta Q^2 - 4\eta^3 \operatorname{sech}^2 \eta q. \tag{4.10}$$

The Hamiltonian describes the energies of the system. When using the centre-of-mass coordinate system, the Hamiltonian can be divided into the center-of-mass energy, E, and the interaction energy, ϵ, such that $H = E + \epsilon$ with these constants of motion, E and ϵ, given by

$$E = \frac{P^2}{4\eta} + \omega^2 \eta Q^2 \tag{4.11}$$
$$\epsilon = \frac{p^2}{\eta} + \frac{\omega^2 \eta q^2}{4} - 4\eta^3 \operatorname{sech}^2 \eta q \tag{4.12}$$

Note that the center-of-mass energy is dependent only on P and Q and the interaction energy is dependent only on p and q.

The centre-of-mass energy, E, considers the relative position of the solitons; it is a function of the position and momentum of the centre-of-mass of the whole system. The interaction energy, ϵ, includes contributions from potential energy, both from the harmonic trap and the interaction potential, and from the overall kinetic energy of the system. When the interaction energy is negative it means the interaction potential is dominating. A strong interaction between the solitons occurs when they are close together and there is an exchange of energy. The faster the exchange of energy between the solitons, the larger and more negative the interaction energy.

As $H = E + \epsilon$, for a given H, the interaction energy corresponds to the centre-of-mass energy, but systems can have both small, both large or one high and one low. The balance of the interaction and centre-of-mass energies is unique for each set of initial conditions. For the Poincaré sections, the centre-of-mass energy is always positive. This means that whenever $E > H$ the interaction energy is negative.

4.4.2 Deriving Poincaré Conditions

Recalling the constants of motion, Equations (4.11) and (4.12), here we express them in terms of $q_1,\ q_2,\ p_1,$ and p_2 for center-of-mass coordinates for solitons of equal mass,

$$E = \frac{(p_1+p_2)^2}{4\eta} + \frac{\omega^2\eta\,(q_1+q_2)^2}{4}, \tag{4.13}$$

$$\epsilon = \frac{(p_1-p_2)^2}{4\eta} + \frac{\omega^2\eta\,(q_1-q_2)^2}{4} + V\,(q_1-q_2)\,, \tag{4.14}$$

where

$$V\,(q_1-q_2) = -4\eta^3\,\mathrm{sech}^2\,\eta\,(q_1-q_2).$$

When we set $q_2=0$, the constants of motion become

$$\begin{aligned} E &= \frac{(p_1+p_2)^2}{4\eta} + \frac{\omega^2\eta q_1^2}{4}, \\ \epsilon &= \frac{(p_1-p_2)^2}{4\eta} + \frac{\omega^2\eta q_1^2}{4} + V\,(q_1)\,. \end{aligned}$$

Taking the sum of these, we obtain the Hamiltonian, $H = E + \epsilon$, which simplifies to give

$$H = \frac{p_1^2}{2\eta} + \frac{p_2^2}{2\eta} + \frac{\eta\omega^2 q_1^2}{2} + V\,(q_1)\,,$$

and rearranging for p_2 we obtain

$$p_2 = \pm\sqrt{2\eta\left[H - \frac{p_1^2}{2\eta} - \frac{\eta\omega^2 q_1^2}{2} - V\,(q_1)\right]}.$$

As $p_2 < 0$ is required, we take only the negative root of p_2^2. Substituting this into the expression for the center-of-mass energy gives

$$\begin{aligned} E &= \frac{p_1^2}{4\eta} + \frac{1}{2}\left[H - \frac{p_1^2}{2\eta} - \frac{\eta\omega^2 q_1^2}{2} - V\,(q_1)\right] - \frac{p_1}{2\eta}\sqrt{2\eta\left[H - \frac{p_1^2}{2\eta} - \frac{\eta\omega^2 q_1^2}{2} - V\,(q_1)\right]} + \frac{\eta\omega^2 q_1^2}{4} \\ &= \frac{1}{2}\left[H - V\,(q_1)\right] - \frac{p_1}{2\eta}\sqrt{2\eta\left[H - \frac{p_1^2}{2\eta} - \frac{\eta\omega^2 q_1^2}{2} + V\,(q_1)\right]}. \end{aligned} \tag{4.15}$$

This expression for the centre-of-mass energy is only dependent on q_1 and p_1 and so we can proceed with the Poincaré section where we compare the dynamics of soliton 1 with this energy.

4.4.3 Interpretation

The Poincaré sections in Figure 4.7 gives the region of possible q_1 and p_1 values for a system with total energy, H. The centre-of-mass energy, E, is represented by the colour scale, with highest energies in red and lowest in blue. Each black contour represents a different centre-of-mass energy which can be determined by initial conditions. The white contour shows the energy level for

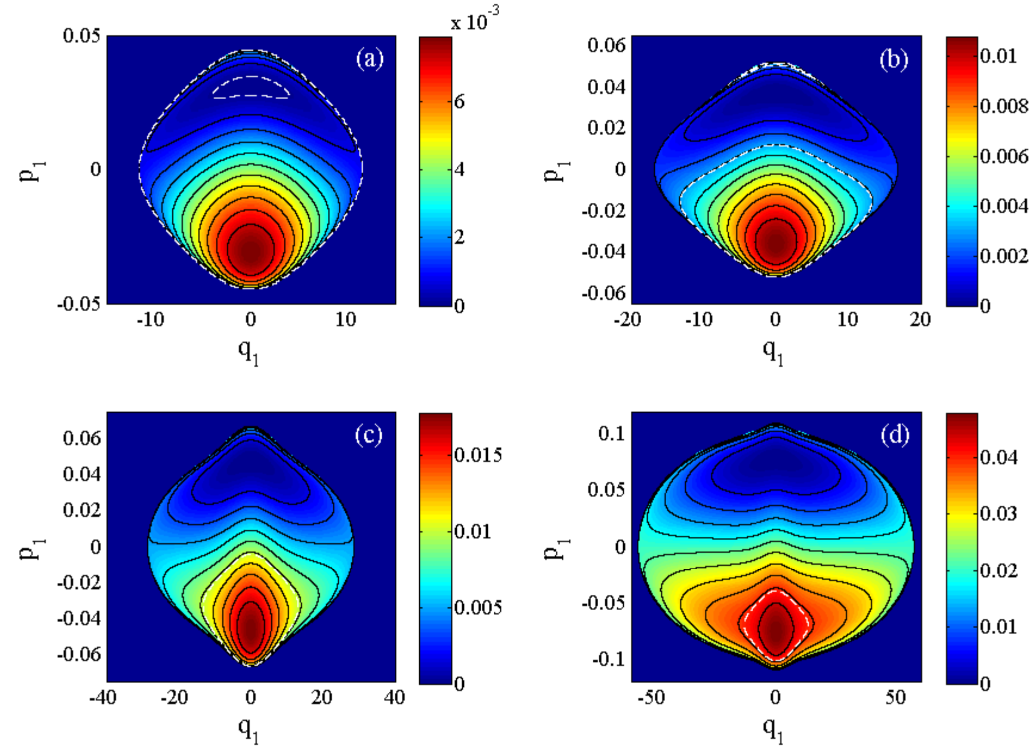

Figure 4.7: Poincaré sections for the two-soliton system with varying total energy levels: (a) $H = 1 \times 10^{-4}$, (b) $H = 3 \times 10^{-3}$, (c) $H = 1 \times 10^{-2}$, (d) $H = 4 \times 10^{-2}$. The white contours indicate the region where $E = H$.

$E = H$. Data points for initial conditions which give a particular E should follow the respective contour exactly.

In Figure 4.7 we examine four Poincaré sections for different values of H. The centre-of-mass energy can exceed the total energy of the system. This is due to the interaction energy ϵ not being considered in the conditions used to plot the Poincaré section, given by Equation (4.15). The regions inside the white contours indicate the instances when $E > H$ and the value of ϵ is negative so the solitons are interacting strongly and there is an exchange of energy.

Examining the sections we see the centre-of-mass energy is high for $p_1 < 0$ and low for $p_1 > 0$. Recalling the conditions set for the contour $(q_2 = 0,\ p_2 < 0)$, we consider the instances when the solitons have similar conditions. When $p_1 < 0,\ \ (p_2 < 0)\,,\ q_1 - q_2 \approx 0$ the solitons are moving through the origin in the same direction and there is a long interaction. When the solitons move together their interaction is large, attractive and negative, and so there is a large centre-of-mass energy, in some cases with $E > H$. This is shown in the Poincaré sections by the higher energy levels shown in the lower halves of the sections. Contrastingly, when the solitons pass each other going in opposite directions $(p_1 > 0,\ p_2 < 0)$, there is a large overall kinetic energy and so the interaction energy is large such that E is small. The white contours indicate the region of values for which $E > H$, $\epsilon < 0$, the interaction between solitons is large and there is an exchange of energy.

We notice how the shape and size of the section varies with the different total energy levels. For a two-soliton system in a harmonic trap, without any interaction, the Poincaré section is a circle. As H is increased, the Poincaré phase space tends to a circular shape, seen in Figure 4.7(d), because for a system without any interaction, the phase space would be a circle. For lower values of H, the section resembles a diamond shape.

For a smaller energy level, the smaller the range of values for q_1 and p_1, as the scale of the system is decreased, the possible regions is reduced. In Figure 4.7(a) the section appears to be stretched upwards with the lower energy contours covering almost half of the section. In (b) we see the diamond shape is more defined with the section almost perfectly symmetrical along the diagonals. The majority of high energy contours still lie in the bottom half of the section but they are more spread than those depicted in (a). This trend continues in (c) as the energy increases. The range of values is greater and the contours are more evenly spread between positive and negative momenta.

In the final case, (d), the contours demonstrate how the high and low energy levels are nearly equal in their coverage of the section. The section is almost a perfect circle in shape; the bump running along the $q_1 = 0$ line is the only discrepancy. The conditions used to define the Poincaré sections specify $q_2 = 0$ and so it is reasonable to assume that the bumps in the section are due to in the interaction between the solitons. It is particularly clear at $q_1 = 0,\ p_1 \approx 0$ when the solitons have the same position coordinate, they occupy the same place and must interact. The contours which include initial momenta around zero show the interaction bump when it is most defined. This agrees with our conclusions that the interaction is more effective and observed clearer when the solitions are travelling slower.

Interestingly it is not immediately clear what effect the interaction is having in the Poincaré sections for the lower energy levels, (a) and (b). When presented along side the higher energy levels of (c) and (d), it is more obvious that the more square forms of (a) and (b) are due to the interaction. This additional potential energy appears to stretch the section up and down but the bumps are not clear at all. We predict that if H is increased further, the bumps at the extremes of p_1 will decrease in magnitude and the section will resemble that of a system without interaction, a perfect circle.

4.4.4 Tracing Contours

Each contour is specific to an individual set of initial conditions. We choose initial conditions, $q_1(0) = 20,\ q_2(0) = -5,\ p_1(0) = p_2(0) = 0$, which allow us to calculate the overall energies of the system. We recall Equations (4.13) and (4.14) and use our initial conditions to obtain

$$E_0 = 1.4 \times 10^{-3} \qquad \text{and} \qquad \epsilon_0 = 3.8 \times 10^{-3}. \tag{4.16}$$

The sum of these give the total energy of the system, $H = 5.1 \times 10^{-3}$, which dictates the shape and size of the Poincaré section.

In compliance with the conditions set on the Poincaré section, we must pick out the values of the simulated data which satisfy $q_2 = 0$ and $p_2 < 0$. Only these data points are relevant for this intersection of the phase space. The other data points exist in other sections but are not needed here. A relatively small number of data points satisfy our conditions so in order to fill the contour we must extend the running time for the model. Setting the maximum time to be $100,000$, the model creates $37,341$ time steps, of which 259 satisfy the conditions and are relevant for the section.

Using conditional statements the times when soliton 2 crosses the origin in a negative direction are recorded. There is a degree of inaccuracy here since the model uses discrete time steps; the statement checks for a crossing point between each time step and, if satisfied, records the earlier time. Methods for decreasing this error include reducing the relative tolerance within the ODE45 solver. Additionally a method of interpolating the times could be applied.

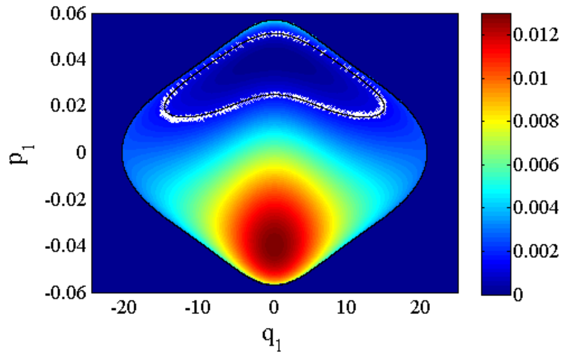

Figure 4.8: Poincaré section for the two-soliton system for $H = 5.1\times10^{-3}$ given by the initial conditions $q_1(0) = 20,\ p_1(0) = 0,\ q_2(0) = -5,\ p_2(0) = 0$. Simulated data points are overlaid in white and follow the black contour.

In Figure 4.8 we notice that the shape of the Poincaré section is similar to that depicted in Figure 4.7(b). The black line highlights the contour mapped for centre-of-mass energy, $E_0 = 1.4\times10^{-3}$ and the white crosses are data points as extracted from the two-soliton model. The data points fill the majority of the contour so we know that the model has been run for a sufficiently long period. The simulated values are consistent with the contour mapped so we are confident that the conditional statements are successfully extracting the correct data points which satisify the Poincaré section conditions.

In this chapter we considered a typical two-soliton system by including the interaction potential in the Hamiltonian. We observed the phase shift which occurred when the solitons collided with sufficiently low momenta. Extending timescales, we saw the trajectories take a sinusoidal shape and considered what might cause this. Varying the initial separation we considered to what extent the different frequencies affected the motion of the solitons. The Poincaré sections offered a visual representation of all possible trajectories a soliton can take in a two-soliton system. There is much more information available on the section when compared to individual simulated trajectories.

Chapter 5

Two-Soliton Dynamics: The Lennard-Jones Potential

In the two-soliton system there are additional forces to consider. The solitons have attractive and repulsive forces between them. The long range attraction is felt when the solitons are far apart; when in close range of each other, the solitons repel. It follows that for any large separation, an attraction is felt between the solitons and they move towards each other. Eventually they come into close enough proximity that they repel each other. Regular particles would move to an equilibrium separation such that the attractive and repulsive forces are equal. This would only happens for solitons if there is dissipation in the system. By the properties of a soliton in Section 1.1, we know that solitons propagate indefinitely, and so they would never come to rest at this equilibrium separation.

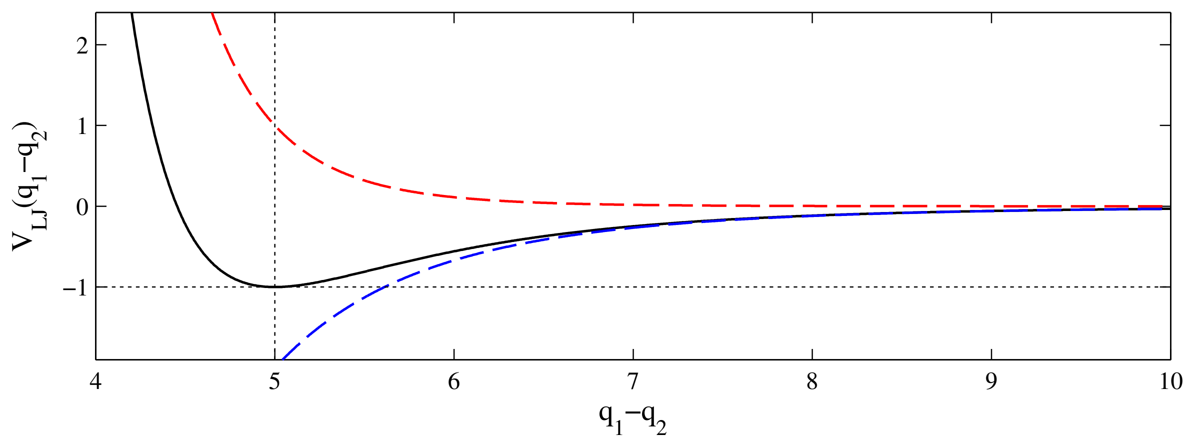

Figure 5.1: Lennard-Jones Potential (black) with $\tau = 1,\ \sigma = 5$. Red dashed line is the attraction term. Blue dashed line is the repulsion term.

The attractive and repulsive forces determine the potential energy of the two solitons. The attractive and repulsive potential energies correspond to the negative and positive terms in Equation (5.1) respectively. The sum of these potentials is called the Lennard-Jones Potential [28],

$$V_{LJ} = \tau \left[\left(\frac{\sigma}{q_1 - q_2} \right)^{12} - 2 \left(\frac{\sigma}{q_1 - q_2} \right)^{6} \right] \tag{5.1}$$

where $q_1 - q_2 = q$ is the separation, σ is the equilibrium separation constant and τ is the depth of the well. The potential is plotted in Figure 5.1 with $\tau = 1$ and $\sigma = 5$. The blue dashed line demonstrates how the potential energy of attraction changes with separation, the red dashed line for the potential energy of repulsion. The black line shows clearly how the total of these potentials becomes the Lennard-Jones potential. The dotted lines highlight the parameters of the potential. The minimum occurs at $q = 5$; this gives the value of σ, the equilibrium separation constant. It is also shown that τ, the depth of the well, is -1. Altering these parameters can affect at what separation the particles become repulsive and to what extent.

The Hamiltonian

As before, we adjust our equation for the Hamiltonian to include the Lennard-Jones potential energy and obtain

$$H = \frac{p_1^2}{2\eta_1} + \frac{p_2^2}{2\eta_2} + \frac{1}{2}\eta_1\omega^2 q_1^2 + \frac{1}{2}\eta_2\omega^2 q_2^2 + \tau\left[\left(\frac{\sigma}{q_1 - q_2}\right)^{12} - 2\left(\frac{\sigma}{q_1 - q_2}\right)^{6}\right]. \tag{5.2}$$

The potential energy which corresponds to the harmonic trap is included. We proceed and calculate Hamilton's equations for the Lennard-Jones potential. We only consider solitons of equal mass.

$$\begin{aligned}
\frac{dq_1}{dt} &= \frac{\partial H}{\partial p_1} \qquad \text{and} \qquad & \frac{dp_1}{dt} &= -\frac{\partial H}{\partial q_1} \\
&= \frac{p_1}{\eta} & &= -\eta\omega^2 q_1 + \frac{12\tau}{q_1 - q_2}\left[\left(\frac{\sigma}{q_1 - q_2}\right)^{12} - \left(\frac{\sigma}{q_1 - q_2}\right)^{6}\right] \qquad (5.3) \\
\frac{dq_2}{dt} &= \frac{\partial H}{\partial p_1} \qquad \text{and} \qquad & \frac{dp_1}{dt} &= -\frac{\partial H}{\partial q_1} \\
&= \frac{p_2}{\eta} & &= -\eta\omega^2 q_2 - \frac{12\tau}{q_1 - q_2}\left[\left(\frac{\sigma}{q_1 - q_2}\right)^{12} - \left(\frac{\sigma}{q_1 - q_2}\right)^{6}\right] \qquad (5.4)
\end{aligned}$$

5.1 Short Term Dynamics

We examine how the Lennard-Jones potential affects the dynamics of a system. We consider a system without the trapping potential with initial separation $q \approx \sigma$. The solitons are placed in an open space with zero momenta. Any motion observed is due to the attractive and repulsive forces within the potential.

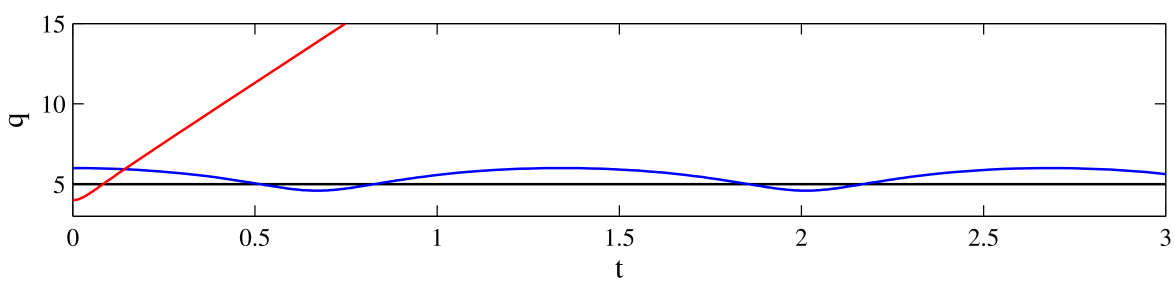

Figure 5.2: A separation - time plot displaying effects of the Lennard-Jones potential in a two-soliton system. The red, black and blue lines are for initial separations $q = 4, 5, 6$ respectively.

In Figure 5.2 the black line represents the stationary trajectory of two solitons positioned with separation $q = \sigma = 5$. With attractive and repulsive forces equal, the solitons remain stationary. The red line shows the trajectory when the solitons are given initial separation $q = 4$. With $q < \sigma$, the repulsive term in the potential forces a sudden repulsion. The blue line represents the motion of the solitons when given initial separation $q = 6$. Starting with $q > \sigma$ the solitons are attracted together but when they cross the black line they feel the repulsion. The oscillation motion in the blue line here occurs as the solitons oscillate in the bowl-like trap at $q = \sigma$ in Figure 5.1. The oscillation is not sinusoidal and demonstrates the uneven strengths in the attractive and repulsive forces. The difference in trajectory between the red and blue lines highlights the unequal gradients of the potential walls around $q = \sigma$ in Figure 5.1.

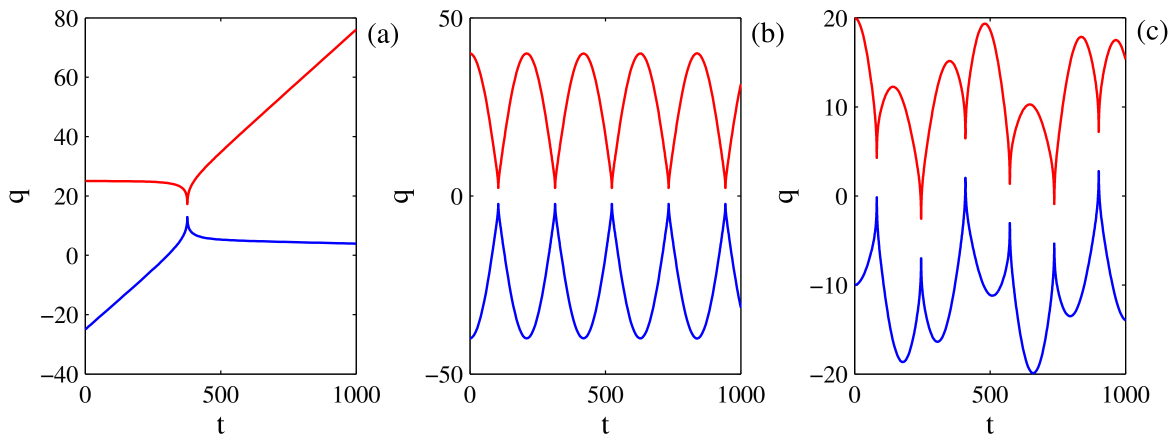

Figure 5.3: Position - time plots for soliton 1 and soliton 2 with initial conditions (a) $q_1(0) = 25,\ p_1(0) = 0,\ q_2(0) = -25,\ p_2(0) = 0.01$; (b) $q_1(0) = 40,\ p_1(0) = 0,\ q_2(0) = -40,\ p_2(0) = 0$; (c) $q_1(0) = 20,\ p_1(0) = 0,\ q_2(0) = -10,\ p_2(0) = 0$. The trap frequency for (b) and (c) is $\omega = 0.014$ as set by Martin *et al.* [19].

Similar to the interaction potential model considered in Chapter 4, we choose our conditions such that we ensure an interaction occurs. To observe the full effects of the Lennard-Jones potential, we consider three specific cases, as shown in Figure 5.3;

(a) Soliton 1 stationary; soliton 2 moves towards the origin without the harmonic trap;

(b) Both solitons released from trap wall symmetrically;

(c) Both solitons released from trap wall asymmetrically.

Given the form of the potential we have certain expectations concerning the behaviour of the solitons. For initial separation $q(0) > 0$, the potential only exists $q > 0$ for all t. We know from the origin of the expression, the solitons repel each other when the separation is sufficiently small, and so we know that the paths of the solitons do not cross.

Figure 5.3 shows the paths of the solitons in the system for each case individually. In case (a) only soliton 2 is initially moving. At $t \approx 300$ the solitons have a separation $q \approx 25$, the long range attraction has an effect and soliton 2 begins moving towards soliton 1. Both solitons accelerate towards each other until $t \approx 380$ when $q = \sigma = 5$ and the repulsion causes both to change direction and accelerate away. Soliton 1 is stationary before the interaction but the repulsion causes the soliton to leave with constant velocity; soliton 2 approaches with speed but the repulsion causes the deceleration, reverses the direction and the soliton leaves with almost no velocity. There is an exchange of kinetic energy between the solitons.

Figure 5.3(b) demonstrates the repulsion occuring at the centre of the trap cleanly. Released from the same height the solitons move towards each other with equal velocity; when the separation reaches $q = \sigma = 5$ the solitons repel each other and travel back up the trap walls. As in cases without any interaction the solitons decelerate to their initial positions, change directions and travel back towards the origin. The long range attraction is not evident here as the solitons move towards each other due to potential energy from the harmonic trap.

In case (c) the solitons are released from different heights on the trap wall and this asymmetricity is reflected in the motions mapped in the plot. The repulsions occur when the solitons have separation $q = \sigma$ but, unlike case (b), this does not happen central in the trap, and this causes the uneven nature of the trajectories. An overall sinusoidal shape appears, similar to those seen in Figure 4.3.

5.2 Longer Term Dynamics

We wish to examine the effect of multiple collisions in the Lennard-Jones system. The long term attraction in the Lennard-Jones potential means that over an extended timescale the solitons would eventually come together, no matter what their initial separation or momenta. However, in order to achieve multiple collisions in the shortest timescale we consider cases in the harmonic trap. Similar to those results explore in Section 4.2 we look at cases with unequal initial conditions; we alter the height from which soliton 1 is released from rest, with soliton 2 stationary at the centre of the trap.

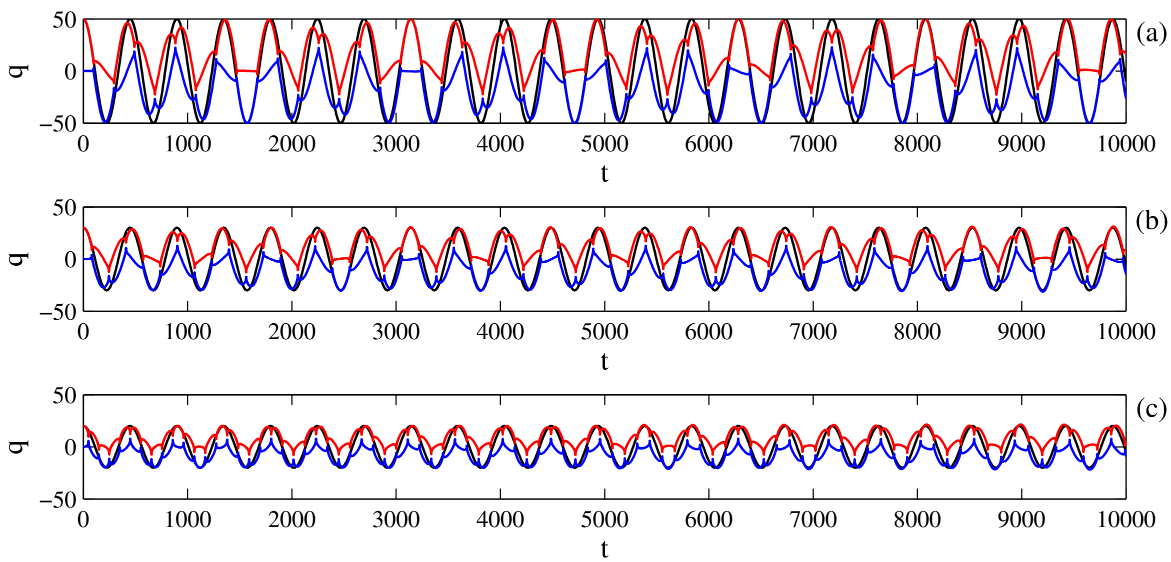

Figure 5.4: Position - time plots for soliton 1 and soliton 2 with initial conditions $q_2(0) = p_1(0) = p_2(0) = 0$ and (a) $q_1(0) = 50$, (b) $q_1(0) = 30$, (c) $q_1(0) = 20$. The black lines indicate the sinusoidal profile of oscillations.

Figure 5.4 gives the trajectories for three cases; in each case we observe the motion of soliton 2 is initiated by the repulsion felt when the solitons are sufficiently close.

A greater initial separation causes a higher difference in velocities when the solitons meet; this causes a more dramatic energy transfer between the solitons. Just considering the separation of the solitons, they always return to their initial separation between repulsions. For systems with smaller initial separations, the energy required to do this is greatly reduced. This makes for a smaller scale of oscillation in the system.

The sinusoidal profile of oscillations witnessed in these longer dynamics for the interaction potential is not as clear for the Lennard-Jones potential. It is not immediately evident in case (a) but is obvious in (c), as indicated by the black lines in Figure 5.4. On inspection, the sinusoidal profile has period $T \approx 450$ in all three cases. This implies a frequency of $\omega = \pi/225 \approx 0.014$, the trap frequency. This frequency observed and the form of the trajectories suggests the sinusoidal form refers to the exchange of energy.

5.3 Frequencies

We explore the other frequencies which occur in the system with the Lennard-Jones potential. As before, we consider the Fourier transform and examine a periodogram. We apply a Fourier transform to separation data, i.e. $q = q_1 - q_2$ (used for Figure 5.5), which we also shift such that the oscillation occurs around the origin. Examining a system without the harmonic trap we obtain the frequency $\omega \approx 6.788$ as shown in Figure 5.5, which we expect to be the frequency of the 'bowl-like' trap in the Lennard-Jones potential.

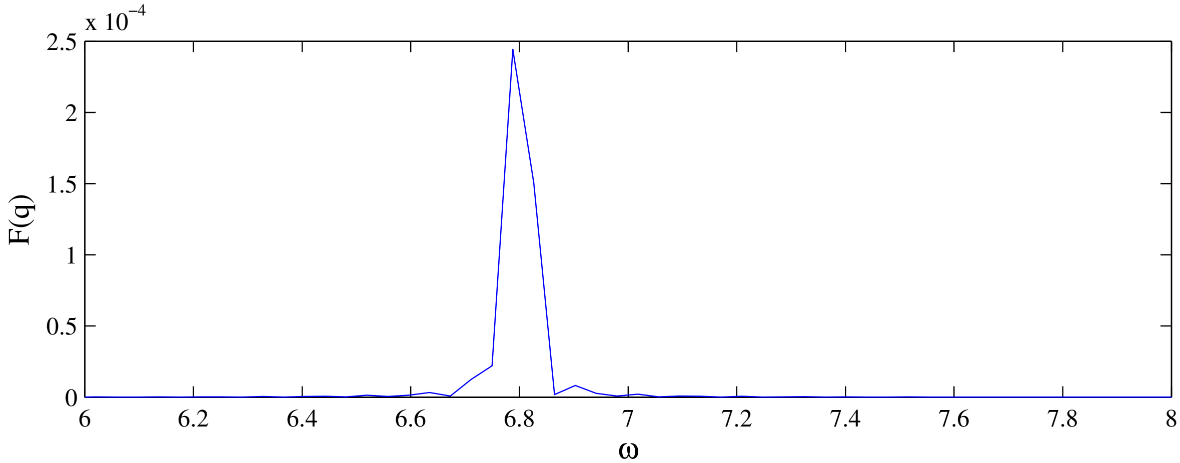

Figure 5.5: Periodogram showing Fourier transform of separation data which extracts the frequency $\omega \approx 6.788$. The case examined has initial conditions $q_1(0) = -2,\ q_2(0) = 2,\ p_1(0) = p_2(0) = 0$, c.f. the blue line in Figure 5.2.

As before, we can also identify frequencies using a Taylor series expansion and apply this to identify the frequency of this bowl. We take a Taylor expansion about $q = \sigma$, to order q^2, and obtain

$$V_{LJ} \approx -\tau \left[1 - 36\frac{\tau}{\sigma^2}\left(q-\sigma\right)^2\right] \tag{5.5}$$

which is shown to be a decent approximation in Figure 5.6.

In Figure 5.6 we see the Lennard Jones potential plotted with the Taylor approximation overlaid. We observe both follow the same curve at the minimum at $q = \sigma = 5$. To identify the frequency, we compare like terms in the Taylor expansion with the harmonic trap term in the

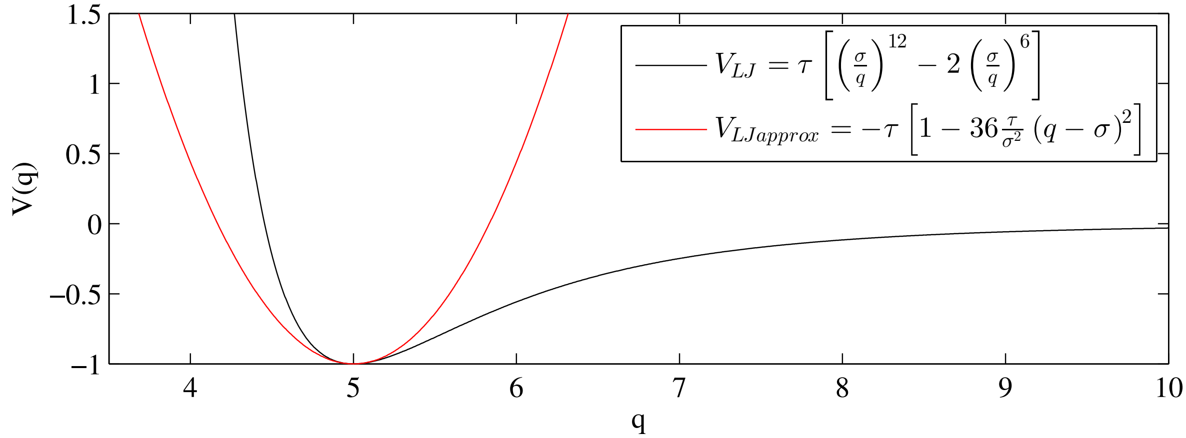

Figure 5.6: Comparison with Taylor Series expansion for the Lennard-Jones Potential Energy.

interaction energy (Equation (4.12)). Comparing the magnitudes of the quadratic terms gives

$$36\frac{\tau}{\sigma^2} = \frac{1}{4}\eta\omega^2$$
$$\implies \omega_{LJ} \approx 6.788$$

This matches the frequency observed in the Fourier transform and so we are satisfied it is the frequency of the trap at $q = \sigma$ in the Lennard-Jones potential. This frequency is significantly larger than the trap frequency and thus in calculating a combined frequency we find that $\omega_{comb} \approx \omega_{LJ}$, since $\omega_{LJ} \gg \omega_{trap}$. So in the instances that the solitons have separation $q \approx \sigma$ and they are in the centre of the trap, the effect of the trap is negligible.

5.4 Poincaré Sections

Following the methods used in Section 4.4, we analyse the complicated dynamics of the two-soliton system using Poincaré sections. We choose the same conditions to create the Poincaré sections, $q_2 = 0,\ p_2 < 0$ to give a unique definition of the intersection of phase space. Adapting Equation (4.15), the expression for the centre-of-mass energy becomes,

$$E = \frac{1}{2}\left\{H - \tau\left[\left(\frac{\sigma}{q_1}\right)^{12} - 2\left(\frac{\sigma}{q_1}\right)^{6}\right]\right\} - \frac{p_1}{2\eta}\sqrt{2\eta\left\{H - \frac{p_1^2}{2\eta} - \frac{\eta\omega^2 q_1^2}{2} + \tau\left[\left(\frac{\sigma}{q_1}\right)^{12} - 2\left(\frac{\sigma}{q_1}\right)^{6}\right]\right\}}. \tag{5.6}$$

The energy is only dependent on q_1 and p_1 and so we proceed with the Poincaré section where we compare the dynamics of soliton 1 with this energy. As before, the interaction energy, ϵ, can be negative when the Lennard-Jones potential is dominant. As the attractive term of the potential (with q^{-6}) is negative, there is a strong interaction between the solitons whilst $q > \sigma$. When $q \approx \sigma$, the repulsive term then dominates the interaction energy and ϵ becomes positive.

5.4.1 Interpretation

The Poincaré sections in Figure 5.7 give the region of q_1 and p_1 values for systems with total energy, H. The colour scale represents the centre-of-mass energy, E. Each black contour represents an individual centre-of-mass energy, relevant for specific initial conditions. The white contour is the energy level for $E = H$. The red contours give the lowest E for each system.

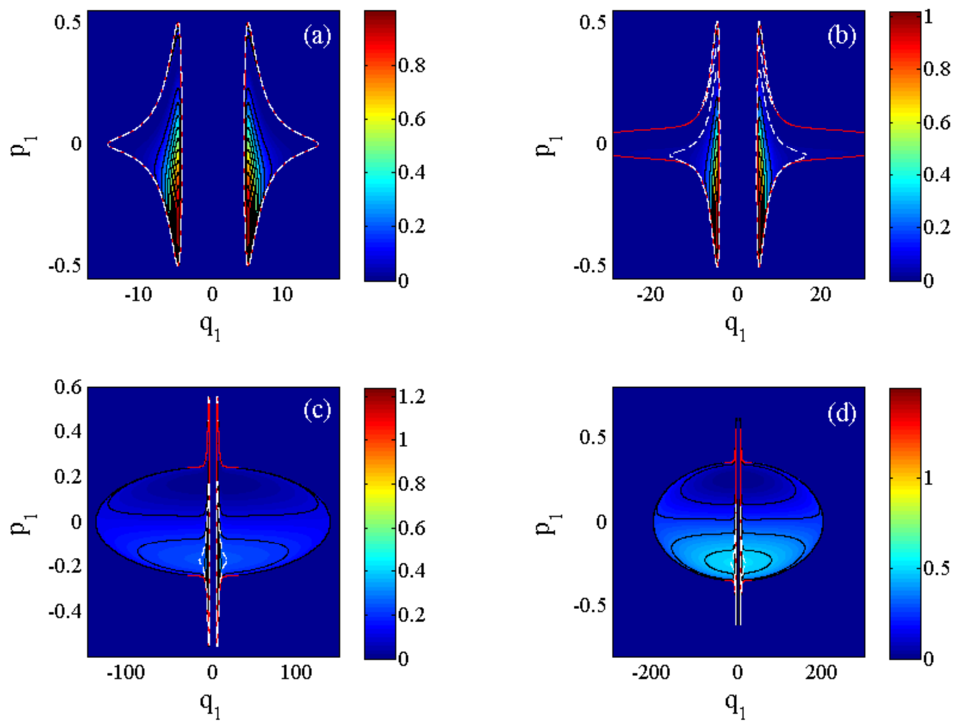

Figure 5.7: Poincaré sections for the two-soliton system with varying total energy levels; (a) $H = 1 \times 10^{-4}$, (b) $H = 2 \times 10^{-2}$, (c) $H = 2.4 \times 10^{-1}$, (d) $H = 5 \times 10^{-1}$. The white contours indicate the region where $E = H$. The red contours show the lowest centre-of-mass energy in each system.

In Figure 5.7 we examine four Poincaré sections for different values of H. As before the energy level affects the range of values for q_1 and p_1 and the spread of the contours. The section does not cover the full range of q_1; we observe the separation gap in the middle showing that the solitons do not ever meet as the repulsive term in the potential ensures when $q_2 = 0$, $q_1 > 5$ or $q_1 < -5$. Every section contains spikes in the extremes of the p_1 axis, with the higher energy levels contained in the lower half when $p_1 < 0$. Consistent with sections given in Figure 4.7, the centre-of-mass energy is high for $p_1 < 0$ when the solitons are moving around the origin in the same direction, and low for $p_1 > 0$ when the directions of motion are opposite. This is not as clear in (c) and (d) but is evident in the lower energy levels of (a) and (b). The red contours indicate the lowest centre-of-mass energy which occurs when the square-root of Equation (5.6) equals zero. These contours give the absolute outline of possible trajectories. These characteristics are consistent throughout the different total energy levels; it is the overall shape and size which changes.

For lower energy levels, shown in (a) and (b), the sections are small, contained and clearly defined. There is an overall diamond shape with spikes at the extremes of q_1 as well. As the energy increases these spikes become more pronounced as the range of q_1 gets bigger. The lower energy contours take up more of the section and are spread higher in the range of p_1.

In (c) and (d) the higher values of H make the area of the lower energy contours much larger and more rounded. The overall shape is more circular, but the separation gap and spikes in the extreme of p_1 remain. The high energy contours are small in the perspective of the plot and the lower ones continue to spread higher up the section.

The most interesting difference is the change from (b) to (c). Despite the difference in energy levels between (a) and (b) being greater, significant change in form is much more evident between (b) and (c). This suggests there may be a critical energy level between these two levels where the system changes dramatically.

As was clear in Figure 4.7, as the total energy of the system is increased, the section becomes more circular in shape. It happens here for the Lennard-Jones potential; the circle is first seen in (b), outlined in red, as an oval. In (d) the section is almost circular, except for the spikes in the extremes of p_1 and the separation gap along $q_1 = 0$. We predict that if H is increased further, the spikes will decrease in magnitude and the section will resemble that of a system without interaction.

These Poincaré sections confirm that the effects of the Lennard-Jones potential are more defined in a system with a lower total energy. This is what we expect since the dynamics of the system are most dramatic when the solitons are close to the separation constant $q \approx \sigma$ and the repulsive and attractive forces have the greatest effect.

5.4.2 Tracing Contours

We are interested in how our simulations fit onto one of the centre-of-mass energy contours. We choose initial conditions for soliton 1, $q_1 = 10,\ p_1 = 0.2$, and soliton 2, $q_2 = 2,\ p_2 = 0.1$, and use these values to calculate the energies of the system. Recalling Equations (4.11) and (4.12) for our conditions, we obtain

$$E_0 = 1.809 \times 10^{-1} \qquad \text{and} \qquad \epsilon_0 = -9.53 \times 10^{-2}. \tag{5.7}$$

The total energy of the system is given by $H = 8.56 \times 10^{-2}$ which determines the form of the Poincaré section. The interaction energy is negative because with these initial conditions the solitons are positioned close together and move in the same direction. The closeness makes the centre-of-mass energy high and the lack of overall kinetic energy makes the interaction energy low; this results in a negative interaction energy.

Applying the same method as in Section 4.4.4, the relevant values for our chosen intersectin of phase space which satisfy $q_2 = 0$ and $p_2 < 0$ are extracted from the simulated data. As before, the running time is extended this time to $50,000$ producing $1,760,873$ time steps, of which 131 are relevant and satisfy the conditions. Note that the relative tolerance level in ODE45 is decreased in order to extract a sufficient number of accurate data points. The conditional statements are applied to extract the times when the trajectory of soliton 1 passes through the section of phase space in the negative direction.

In Figure 5.8 shows the two-soliton system with an energy level set by the initial conditions which lies between the values used in Figure 5.7 (b) and (c). The entire section is not visible in the plot, instead the relevant area is shown. The black line highlights the contour for the centre-of-mass energy, $E_0 = 1.809 \times 10^{-1}$ and the white crosses are the data points as extracted from the two-soliton model.

The data points match the contour on the positive side of the section for a system with $q_1 > q_2$. Since our conditions have set $q_2 = 0$ it follows that $q_1 > 0$. To obtain data to match the contour

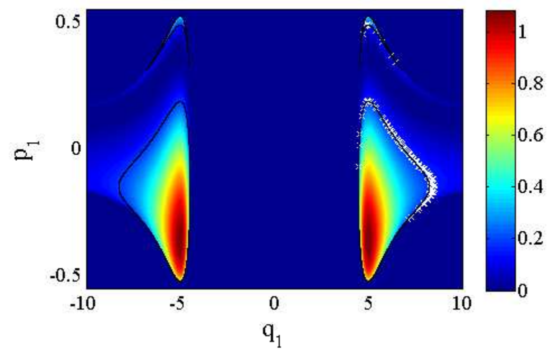

Figure 5.8: Poincaré section for the two-soliton system with the Lennard-Jones potential for $H = 8.56 \times 10^{-2}$ given by initial conditions $q_1(0) = 10,\ p_1(0) = 0.2,\ q_2(0) = 2,\ p_2(0) = 0.1$. Simulated data points are overlaid in white and follow the black contour.

for the negative side the initial conditions should be altered such that $q_1 < q_2$. It is not possible to have data points to appear for both sections from the same two-soliton model as the solitons never cross. The points fill the majority of the contour; an extended timescale would fill the whole contour. The points do not lie cleanly on the contour even though the tolerance level has been reduced. It is likely that if the timescale is increased the tolerance should be reduced again.

The contours shown in the Poincaré sections for the Lennard-Jones potential are split, unlike those for the interaction potential. The centre-of-mass energy level highlighted in Figure 5.8 is disjointed with two contours appearing; a main one following the general form of the section and an additional contour at the top with $p_1 \approx 0.5$. This differs from the complete form of the contours on the sections for the interaction potential.

In this chapter we have analysed a two-soliton system which considers the Lennard-Jones potential. Having adapted Hamilton's equations we examined the short term effects of the potential, observing the repulsion and attraction when the separation of the solitons is $q \approx \sigma$, and found the frequency of the potential at this point. Extending the simulations we considered the effects of adding the harmonic trap and varying the initial separation. Poincaré sections allowed us to consider similar systems with different energy levels. This proved important as the form of the sections was unusual and we gained better understanding for choosing suitable conditions for the system. Throughout we have compared these results to those obtained in Chapter 4.

Chapter 6

Summary

In this dissertation we introduced the concept of solitons and Bose-Einstein condensates and discussed how these can be used to model nonlinear systems. We considered the Gross-Pitaevskii equation, examined the time-independent form and derived a soliton solution for one dimension. Whilst full computational modelling of the GPE could have been used, we applied Hamiltonian mechanics to systems which considered the soliton as a particle. We modelled a single soliton in a harmonic trap and observed simple harmonic motion as expected, validating the MATLAB model. Following the work by Marchant *et al.* [18], we introduced a barrier into the trap, examined the dynamics as the barrier height was varied, and found good agreement with the experimental data. Introducing a second soliton, we looked at systems which accounted for the interaction potential and the Lennard-Jones potential separately. The classic interaction potential caused the phase shift to occur when the solitons collided with sufficiently low momenta. We compared the effects of the interaction potential frequency with the trap frequency by varying the initial separation. In the Lennard-Jones potential system, we observed the solitons repel when in close proximity. We found the frequency of the Lennard-Jones potential and compared its effects with the trap frequency. In both systems we used Poincaré sections to enable further understanding of the motion of the two solitons. The sections illustrated all possible trajectories and provided much more information than that offered from individual simulations.

As an extension to this dissertation, two-soliton systems which take into account both the Lennard-Jones and the interaction potentials could be considered. The relative strengths of the potentials are unknown and it would be interesting to see how this would affect the dynamics of the solitons. Increasing the number of solitons in the system would complicate the dynamics; chaotic dynamics in a three-soliton system have been observed by Martin *et al.* [19] and it would be interesting to consider a the Lennard-Jones potential in a three-soliton system.

References

[1] Russell J. *Report on waves: made to the meetings of the British Association in 1842-43*. 1845.

[2] Russell J, Robison J. *Report of the Committee on Waves: appointed by the British Association at Bristol in 1836*.

[3] Drazin PG, Johnson RS. *Solitons: An Introduction*, vol. 2. Cambridge University Press, 1989.

[4] Lonngren K, Scott A. *Solitons in Action*. Academic Press Inc: New York, 1978.

[5] Zabusky NJ, Kruskal MD. Interaction of solitons in a collisionless plasma and the recurrence of initial states. *Phys. Rev. Lett* 1965; **15**(6):240–243.

[6] Korteweg D, De Vries G. On the change of form of long waves advancing in a rectangular canal, and on a new type of long stationary waves. *The London, Edinburgh, and Dublin Philosophical Magazine and Journal of Science* 1895; **39**(240):422–443.

[7] Hasegawa A, Tappert F. Transmission of stationary nonlinear optical pulses in dispersive dielectric fibers. I. Anomalous dispersion. *Applied Physics Letters* 2003; **23**(3):142–144.

[8] Hasegawa A, Tappert F. Transmission of stationary nonlinear optical pulses in dispersive dielectric fibers. II. Normal dispersion. *Applied Physics Letters* 2003; **23**(4):171–172.

[9] Commission on Physical Sciences M, Mathematics P, Council N, Board N, Sciences D. *Nonlinear Science*. Compass series.

[10] Heisenberg W. Über den anschaulichen inhalt der quantentheoretischen kinematik und mechanik. *Zeitschrift für Physik* 1927; **43**(3-4):172–198.

[11] Cornell E. Very cold indeed: The nanokelvin physics of Bose-Einstein condensation. *National Institute of Standards and Technology, Journal of Research* 1996; **101**(4):419–434.

[12] Einstein A. Quantentheorie des einatomigen idealen gases. 2. *Sitzungsberichte der Preußischen Akademie der Wissenschaften* 1925; .

[13] Anderson MH, Ensher JR, Matthews MR, Wieman CE, Cornell EA. Observation of Bose-Einstein condensation in a dilute atomic vapor. *Science* 1995; **269**(5221):198–201.

[14] Ketterle W, Durfee D, Stamper-Kurn D. Making, probing and understanding Bose-Einstein condensates. *arXiv preprint cond-mat/9904034* 1999; **5**.

[15] Billam T, Marchant A, Cornish S, Gardiner S, Parker N. Bright solitary matter waves: formation, stability and interactions. *Spontaneous Symmetry Breaking, Self-Trapping, and Josephson Oscillations*. Springer, 2013; 403–455.

[16] Khaykovich L, Schreck F, Ferrari G, Bourdel T, Cubizolles J, Carr LD, Castin Y, Salomon C. Formation of a matter-wave bright soliton. *Science* 2002; **296**(5571):1290–1293.

[17] Strecker KE, Partridge GB, Truscott AG, Hulet RG. Formation and propagation of matter-wave soliton trains. *Nature* 2002; **417**(6885):150–153.

[18] Marchant A, Billam T, Wiles T, Yu M, Gardiner S, Cornish S. Controlled formation and reflection of a bright solitary matter-wave. *Nature communications* 2013; **4**:1865.

[19] Martin A, Adams C, Gardiner S. Bright solitary-matter-wave collisions in a harmonic trap: Regimes of solitonlike behavior. *Phys. Rev. A* ; **77**(1).

[20] Gross E. Unified Theory of Interacting Bosons. *Phys. Rev.* 1957; **106**:161.

[21] Ginzburg V, Pitaevskii L. On the Theory of Superfluidity. *Sov. Phys. JETP* 1958; **7**:858.

[22] Martin A. Theoretical Studies of Bright Solitons in Trapped Atomic Bose-Einstein Condensates. PhD Thesis, Durham University 2008.

[23] Parker N. Quantum Gases. MAS8114: Topics In Modern Applied Mathematics 2012/13.

[24] Gignoux C, Silvestre-Brac B. *Solved problems in Lagrangian and Hamiltonian mechanics*. Springer, 2009.

[25] Maki J, Kodama T. Phenomenological quantization scheme in a nonlinear Schrödinger equation. *Phys. Rev. Lett.* 1986; **57**(17):2097.

[26] Rafat M, Wheatland M, Bedding T. Dynamics of a double pendulum with distributed mass. *American Journal of Physics* 2009; **77**(3):216–223.

[27] Korsch HJ, Jodl HJ, Hartmann T. *Chaos: a program collection for the PC*. Springer Publishing Company, Incorporated, 2008.

[28] Atkins P, de Paula J, Friedman R. *Physical Chemistry: Quanta, Matter, and Change*.